Convective heat transfer enhancement: effect of multi-frequency heating

Nirmal Kumar Manna and Nirmalendu Biswas
Department of Mechanical Engineering, Jadavpur University, Kolkata, India, and

Pallab Sinha Mahapatra
Department of Mechanical Engineering, Indian Institute of Technology, Chennai, India

Abstract

Purpose – This study aims to enhance natural convection heat transfer for a porous thermal cavity. Multi-frequency sinusoidal heating is applied at the bottom of a porous square cavity, considering top wall adiabatic and cooling through the sidewalls. The different frequencies, amplitudes and phase angles of sinusoidal heating are investigated to understand their major impacts on the heat transfer characteristics.

Design/methodology/approach – The finite volume method is used to solve the governing equations in a two-dimensional cavity, considering incompressible laminar flow, Boussinesq approximation and Brinkman–Forchheimer–Darcy model. The mean-temperature constraint is applied for enhancement analysis.

Findings – The multi-frequency heating can markedly enhance natural convection heat transfer even in the presence of porous medium (enhancement up to ∼74 per cent). Only the positive phase angle offers heat transfer enhancement consistently in all frequencies (studied).

Research limitations/implications – The present research idea can usefully be extended to other multi-physical areas (nanofluids, magneto-hydrodynamics, etc.).

Practical implications – The findings are useful for devices working on natural convection.

Originality/value – The enhancement using multi-frequency heating is estimated under different parametric conditions. The effect of different frequencies of sinusoidal heating, along with the uniform heating, is collectively discussed from the fundamental point of view using the average and local Nusselt number, thermal and hydrodynamic boundary layers and heatlines.

Keywords Natural convection, Heat transfer enhancement, Sinusoidal heating, Heatlines, Porous cavity, Thermal boundary layer, Velocity boundary layer

Paper type Research paper

Nomenclature

A = sinusoidal amplitude of heating (K);
Da = Darcy number;
f = spatial frequency of heating;
F_C = Forchheimer coefficient;
g = acceleration because of gravity (ms^{-2});
I = dimensionless amplitude of heating;
K = permeability of porous medium (m^2);
L = height, length scale (m);
Nu = average Nusselt number;
p = pressure (Pa);

P = dimensionless pressure;
Pr = Prandtl number;
Ra = Rayleigh number;
Ra_m = Darcy–Rayleigh number;
t = time (s);
T = temperature (K);
u, v = velocity components (ms^{-1});
U, V = dimensionless velocity components;
x, y = Cartesian coordinates (m); and
X, Y = dimensionless coordinates.

Greek symbols
α = thermal diffusivity $(\text{m}^2\text{s}^{-1})$;
β = volumetric thermal expansion coefficient of fluid (K^{-1});
δ_v = velocity boundary thickness;
δ_t = thermal boundary thickness;
ε = porosity;
θ = dimensionless temperature;
η = heat transfer parameter;
ν = kinematic viscosity $(\text{m}^2\text{s}^{-1})$;
Π = dimensionless heatfunction;
ρ = density (kgm^{-3});
τ = dimensionless time;
ϕ = phase deviation angle; and
ψ = dimensionless streamfunction.

Subscripts
a = ambient;
h = hot wall;
c = cold wall; and
m = mean.

1. Introduction

In the field of thermal applications, the methodology of heating plays a vital role in the performance and sizing of a system/device. Natural convection or thermal convective flow is found to exist in numerous systems and devices of many disciplines of engineering, science and technology. Electronic devices, solar thermal systems, geothermal energy systems, nuclear waste management, chemical equipment, oil and gas production, food (or grain) processing (or storage), pharmaceutical systems, medical science and biological systems are just a few names in this context. On the era of high-speed digital communication and computation, fast and efficient heat removal from electronic devices is required (Garimella *et al.*, 2016; Kheirabadi and Groulx, 2016). On the other hand, continual investigation on cooling management for the components and systems of electronic and electrical appliances has been going on from the past decades to present time (Nagendran *et al.*, 2015; Kota *et al.*, 2012; Zhao, 2012; Banerjee *et al.*, 2008; Calcagni *et al.*, 2005; Sharif and Mohammad, 2005; Remsburg, 2001; Papanicolaou and Gopalakrishna, 1995; Due and Bilgen, 1990; Incropera, 1988; Bar-Cohen, 1987). Heating is another issue in many applications such as solar collector (Bahrehmand and Ameri, 2015), solar chimney (Haghighi and Maerefat, 2014), solar crop dryer (Sekyere *et al.*, 2016) and room heating. The present date of some medical treatments

(Khanafer *et al.*, 2003; Khaled and Vafai, 2003) demands the thorough knowledge of thermal convection in porous medium as the body tissues behave like porous substance (Khaled and Vafai, 2003). Miniaturization of devices essentially demands the enhanced heat transfer for a thermal system.

Earlier studies and reviews on the thermal convective systems are classically presented in Ostrach (1988), Narasimham (2010), Baïri *et al.* (2014), Öztop *et al.* (2015), Das *et al.* (2017) and in many other works. Theoretically, the heat transporting capacity of natural convection is found to be lowest compared to other convective methods such as forced or mixed convection. Thus, the performance of devices that solely depends on natural convection becomes limited. It inspires to carry out the present numerical work using multi-frequency heating in a fundamental way, in the direction of heat transfer enhancement for a pure natural convection system considering classical geometry.

Enhancing heat transfer under natural convection is of immense challenge from industrial and energy perspectives. To improve heat transfer during natural convection, several basic means and methods are used in earlier works. For examples, a number of works have been performed using cavities with adiabatic block (Kalidasan *et al.*, 2016; Mahapatra *et al.*, 2013; Bhave *et al.*, 2006; Datta *et al.*, 2016), conducting baffle (Tasnim and Collins, 2004) or partitions (Zhang *et al.*, 2016; Selimefendigil and Öztop, 2016). The previous works have also been executed by changing the size of heating body (Biswas *et al.*, 2016a, 2016b, 2016c), the position of heating wall(s) (Valencia and Frederick, 1989), the shape of cavity/wall (u-shaped cavity or wavy wall) (Cho *et al.*, 2012a; Cho *et al.*, 2012b; Parvin and Chamkha, 2014) and the type of heating (Kwak *et al.*, 1998; Anothe and Lage,1996; Mahapatra *et al.*, 2015; Ghalambaz *et al.*, 2017; Tagawa and Ozoe, 1997; Kasayapanand and Kiatsiriroat, 2009). Instead of pure fluid, nanofluids (Meng *et al.*, 2016; Khanafer *et al.*, 2003; Oztop *et al.*, 2011; Chamkha and Rashad, 2012; Chamkha *et al.*, 2015; Kalidasan *et al.*, 2016) are used. However, most of the above methods have reported limited amount of heat transfer augmentation under natural convection. Brief details of heat transfer enhancement along with the means/method and parameters used are indicated in the following Table I.

In the present work with multi-frequency heating, porous medium is considered in the cavity so that the positive outcome from this investigation could implicitly be applicable to clear domain also. It is expected that, in the absence of flow-resisting materials in the same cavity and boundary conditions, the order of heat transfer augmentation in clear-domain is to be relatively higher (than that of porous system). The consideration of porous-medium filled thermal system is vital from the application point of view (Sivasankaran and Bhuvaneswari, 2013; Deng and Chang, 2008; Saravanan and Sivaraj, 2011; Ramakrishna *et al.*, 2013; Wu *et al.*, 2016; Khandelwal *et al.*, 2012; Ismael *et al.*, 2014a; Sheremet and Pop, 2014; Varol *et al.*, 2008; Sarris *et al.*, 2002; Saeid, 2005; Chamkha, 2002; Chamkha and Khaled, 2000; Lauriat and Prasad, 1989). Quantitative heat transfer enhancements in porous substances are found to be limited in these earlier works. In the present problem, the consideration of multiple frequencies and different phase angles of sinusoidal heating (along with the bottom wall) is included for the analysis of heat transfer enhancement with the constraint of same mean-temperature of heating.

The present work differs in a great extent from the previous works on sinusoidal heating reported by many authors as found in Sivasankaran and Bhuvaneswari (2013), Deng and Chang (2008), Wu *et al.* (2016), Sheremet and Pop (2014) and Sarris *et al.* (2002) including sinusoidal heating at bottom wall as reported in Saravanan and Sivaraj (2011), Ramakrishna *et al.* (2013), Khandelwal *et al.* (2012), Sheremet and Pop (2014) and Saeid (2005). The temperature constraint for assessing thermal performance is not applied in

Means/methods	Configuration/conditions	Enhancement in % as reported in the references
Adiabatic square block	An adiabatic block of varying sizes is placed centrally in a differentially heated square cavity (DHC) where Pr = 0.071, 0.71 and 7.10 and Ra = 10^3–10^6	~3% for Pr = 0.71 (Mahapatra et al., 2013) ~10% for Pr = 0.071 (Bhave et al., 2006)
Adiabatic square block	Similar configuration as above but fluid-saturated porous medium is considered in search for heat transfer enhancement using Pr = 0.71, 151, 6450; Da = 10^{-2}–10^{-6}; and Ra_m = 1–10^4	~7% for Pr = 0.71 (Datta et al., 2016)
Protruded bottom heater	Located in a rectangular cavity, with the constraint of fixed perimeter of the heater; using various heater aspect-ratios, Ra = 10^3–10^6 and air, water and ethylene glycol (Pr = 0.71, 5.77, 25.83, 164.5)	~6.2-15% (Biswas et al., 2016a, 2016b, 2016c)
Conducting partitions	In DHC, twin conducting partitions (total length = 0.5 − 0.9, width = 0.01 − 0.2) supported vertically from horizontal adiabatic wall at various positions. Used thermal conductivity ratio = 10^{-4}–10^2, Ra = 10^3–10^6 and Pr = 0.72	~3.67-49.78% (Zhang et al., 2016)
Conducting baffle	The thin baffle (of varying length and position) attached to the left hot wall of DHC is simulated for air at Ra = 10^3–10^5	~31.46% for Ra = 10^4 (Tasnim and Collins, 2004)
An oscillating fin	Located in DHC on left hot wall. Fin length = 0.1-0.4, oscillating amplitude = 0.001-0.1, oscillating period = 0.01-1, thermal conductivity ratio (fin to fluid) = 1-1000, air (Pr = 0.71), Ra = 10^4–10^7	~40% for Ra = 10^6 (Ghalambaz et al., 2017)
Alternately active bi-heater	Flushed on the lower surface of a cavity using heater width = 0.2, air (Pr = 0.71), Ra = 10^3–10^6, dimensionless switchover time-period = 10^{-5}–0.8	~8.4-37.7% (Mahapatra et al., 2015, 2016)
Pulsating heating	Used square cavity with sinusoidally-varying temperature, Pr = 0.7 and Ra = 10^7. The maximum gain noted at the resonance frequency	~−13.1% (Kwak et al., 1998)
Magnetic field	Used liquid metal (Pr = 0.025) in a cubical enclosure, external magnetic field (Hartman number, Ha = 0–1000) and Ra = 10^5 and 10^6	~5% at Ra = 10^5, Ha = 50 and ~9% at Ra = 10^6, Ha =100 (Tagawa and Ozoe, 1997)
Pulsating heating	Used water-filled enclosure, Ra = 2.5×10^8–1.0×10^9, heating period = 20 − 1600 seconds for the experiment	~20% at Ra = 10^9, period = 426 s (Anothe and Lage, 1996)

(*continued*)

Table I.
Brief description of means/methods and heat transfer enhancement during natural convection

Means/methods	Configuration/conditions	Enhancement in % as reported in the references
Nanofluids and partition	Used a cavity with a conducting partition providing Al_2O_3-water and CuO-water nanofluids in different chambers, solid volume fraction (0–0.04), thermal conductivity ratio (0.01–10), Gr = 10^3–10^6	~14.11% (Selimefendigil and Öztop, 2016)
Nanofluid, and varying heating	Used square cavity, sinusoidal heating (amplitude = 0–1, frequency = 0.1–200), Cu-water nanofluid (solid volume fraction ϕ = 0–0.2), Ra = 10^4–10^6	~10% at 10^6 and ϕ = 0.05 (Meng *et al.*, 2016)
Nanofluid, varying heating and twin blocks	Used square cavity, twin diagonal adiabatic blocks, time-varying sinusoidal bottom heating (period = 0.001-0.8), Cu-water nanofluid, Ra = 10^4–10^6	~11% (Kalidasan *et al.*, 2016)
Nanofluid and Magnetic field	Used inclined square cavity (inclination = 0–90°) with sinusoidal cold wall, uniform magnetic field, Cu-water (solid volume fraction ϕ = 0.06), Ra = 10^3–10^5	~18-27.5% (Sheikholeslami *et al.*, 2014)
Nanofluid and varying heating	Used inclined square cavity, sinusoidal heating and cooling, Al_2O and TiO_2 nanofluids (solid volume fraction ϕ = 0–0.1), Ra = 10^3–10^5	~15% for Al_2O at 10^3, ϕ = 0.05 and ~5% for TiO_2 at 10^5, ϕ = 0.05 (Oztop *et al.*, 2011)

Table I.

these works. Except our earlier work on mixed convection in two-sided lid-driven cavity (Biswas *et al.*, 2016a, 2016b, 2016c), the consideration of constant mean-temperature of heating is found only in the work of Saeid (2005). He examined natural convection applying temperature variation sinusoidally about a constant temperature higher than the temperature of cold top wall. The main focus of the present work is to explore the heat transfer augmentation from multi-frequency sinusoidal heating during natural convection in a cavity. For the proper assessment of heat transfer, the temperature variation is defined on the constraint of constant mean-temperature of heating. Under different conditions of sinusoidal heating (consisting of various frequency, amplitude and phase angle), the constant mean-temperature of heating is assumed to be more appropriate for the better heat transfer assessment. The characteristics of the fluid and heat flow dynamics under the multi-frequency heating is more complex. Therefore, several natural questions can be asked to understand the phenomena in the cavity adequately: What happens in the cavity with the multi-frequency heating compared to the uniform heating? What will be the effects of amplitude variation, frequency variation, phase angle variation or Darcy–Rayleigh number variation? How does fluid-flow take place over the hot bottom wall? How does heat flow from the heat source at bottom to the heat sink at sides? How does local Nusselt number vary along the bottom wall? What will be boundary layer thicknesses? How much heat transfer can be enhanced, etc.? The answers for all these questions are thoroughly addressed in this work. The insight of augmentation of thermal energy transport is addressed in great details in this work using heatlines, velocity and thermal boundary layers. The whole work is

arranged in five sections: introduction (Section 1), problem formulation (Section 2), code validation (Section 3), results and discussion (Section 4) and conclusions (Section 5).

2. Problem formulation and numerical procedure
To investigate the impact of multi-frequency heating on natural convection in cavity, the present work considers a two-dimensional flow in a square porous cavity heated non-uniformly through its bottom side. The corresponding problem configuration is presented in Figure 1(a). The heating is provided in such a way that the average temperature (T_m) of bottom wall remains always constant. The other sides of the cavity are: top wall adiabatic and sidewalls cold. The vertical walls are used for cooling with the surrounding ambient that assumes to have a constant temperature T_c (such that $T_m > T_c$). All walls of the cavity are considered impermeable and stationary. The singularity issue of sudden change in temperature at the bottom corners is avoided by inserting insulation patches in the junctions.

To fulfill the mean-temperature constraint, the sinusoidal temperature on the bottom wall (T_h) is applied, which is described by:

$$T_h = T_m + A \sin \left(2\pi f\, x/L \pm \phi \right) \tag{1}$$

where, A, f and ϕ stand respectively for amplitude, spatial frequency and phase angle of the sinusoidal temperature of heating [as depicted in Figure 1(b)] , and L is the dimension of the square cavity. Through a simple integration, the mean temperature (T_m) of bottom heating is defined by:

$$\overline{T}_h = \int_{x=0}^{L} T_h dx/ \int_{x=0}^{L} dx = \frac{1}{L} \int_{x=0}^{L} [T_m + A \sin(2\pi f x/L \pm \phi)]dx = T_m \tag{2}$$

That results to a constant temperature which is the same as the temperature of isothermal heating, irrespective of the parameters of sinusoidal heating. For this reason, the mean
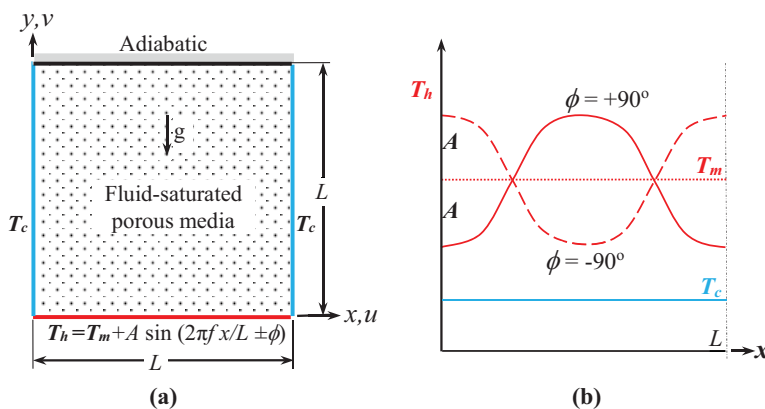
Notes: (a) Problem geometry; (b) sinusoidal temperature profiles for heating along the bottom wall

temperature of heating is chosen as the basis of comparison of different kinds of heating. The temperature of the heating wall under uniform heating condition is assumed to be constant (T_m). When variable heating is provided, the temperature variation along the heating wall takes place. To understand the impact of uniform and non-uniform heating, uniform (or constant) temperature along the bottom wall is considered for uniform heating; and sinusoidal variation of temperature is taken for non-uniform heating. The sinusoidal temperature profile further depends on the amplitude (A) and phase angle (ϕ). By adjusting these parameters (A, ϕ), the spatial distribution of the temperature along the bottom wall of the cavity can be varied and controlled in a sinusoidal manner. The temperature of fluid layer adjacent to this heating wall will severely be affected by the variable temperature of the bottom wall. As a result of this, the characteristics of the flow dynamics become totally different than that of uniform temperature of heating. The complexity in thermo-fluid flow behavior arises because of multi-frequency heating.

The thermo-fluid flow in the cavity is modeled by applying the conservation principles of mass, momentum and energy, and Boussinesq approximation. Both fluid and porous substance are considered continuum and the porous substance is non-deformable. The flow is assumed to be unsteady laminar flow of incompressible Newtonian fluid. The buoyancy force acts vertically upward (opposite to g, as shown in the figure) and is modeled by the Boussinesq approximation. The thermo-physical properties (ρ, ν, α, β) of the working fluid (air of Pr = 0.71) are taken constant. The homogeneous and isotropic nature in porous medium is assumed for adopting Brinkman–Forchheimer–Darcy model (BFDM) with local thermal equilibrium (LTE) (Nield and Bejan, 2006). The model (BFDM) takes care the inertial friction at higher velocity. LTE model considers the same temperature for both solid phase (porous medium) and fluid phase. It simplifies mathematical treatment and saves computational times. This model is suitable when the temperature difference between the solid and fluid phases is small. It can happen in absence of heat generation (or absorption) or high temperature gradient. For the present problem on buoyancy driven flow within the validity of Boussinesq approximation and laminar flow, LTE model is assumed to be appropriate. More details about the model can be found in Pop and Ingham (2002), Hwang and Yang (2012), Kim and Jang (2002) and Zhang and Liu (2008). The insignificant contribution of viscous dissipation is ignored (Ismael et al., 2014b). The assumptions and models, which are used for the present study, are found in many earlier works such as in Sivasankaran and Bhuvaneswari (2013) and Saeid (2005).

The present study is conducted in terms of a group of dimensionless numbers, namely, Prandtl, Darcy and Darcy–Rayleigh number (in short, Pr, Da and Ra_m, respectively) those are defined by:

$$\mathrm{Pr} = \frac{\nu}{\alpha}, \; \mathrm{Da} = \frac{K}{L^2} \text{ and } \mathrm{Ra}_m = \frac{g\beta(T_h - T_c)LK}{\nu\alpha} \tag{3}$$

The permeability (K) of porous medium is addressed by the Darcy number (Da). The porous substance is evenly saturated in the working fluid of Pr = 0.71. Through the parameter of Ra_m, the different strength of thermal convection in the porous cavity is simulated. For the non-dimensionalization of the flow-governing equations, the cavity height L is chosen as length scale. Using both thermal diffusivity and length scale, the velocity scale (α/L) is defined. The pressure (p) and the time (t) are scaled using these length and velocity scales. The temperature difference ($T_m - T_c$) is used to define the non-dimensional temperature. The resulting dimensionless variables for position (X, Y), velocity (U, V), pressure (P), temperature (θ) and time (τ) are respectively described by:

$$(X, Y) = \frac{(x, y)}{L}, \ (U, V) = \frac{(u, v)}{\alpha/L}, P = \frac{(p + \rho gy) - p_a}{\rho(\alpha/L)^2}, \ \theta = \frac{T - T_c}{T_m - T_c}, \ \text{and} \ \tau = \frac{t}{L^2/\alpha} \qquad (4)$$

Accordingly, the transformed set of dimensionless governing equations are expressed by:

$$\frac{\partial U}{\partial X} + \frac{\partial V}{\partial Y} = 0 \qquad (5)$$

$$\frac{\partial U}{\partial \tau} + \frac{1}{\varepsilon^2}\left(U\frac{\partial U}{\partial X} + V\frac{\partial U}{\partial Y}\right) = -\frac{\partial P}{\partial X} + \frac{\text{Pr}}{\varepsilon}\left(\frac{\partial^2 U}{\partial X^2} + \frac{\partial^2 U}{\partial Y^2}\right) - \frac{\text{Pr}}{\text{Da}}U - \frac{F_C\sqrt{U^2 + V^2}}{\sqrt{\text{Da}}}U \qquad (6)$$

$$\frac{\partial V}{\partial \tau} + \frac{1}{\varepsilon^2}\left(U\frac{\partial V}{\partial X} + V\frac{\partial V}{\partial Y}\right) = -\frac{\partial P}{\partial Y} + \frac{\text{Pr}}{\varepsilon}\left(\frac{\partial^2 V}{\partial X^2} + \frac{\partial^2 V}{\partial Y^2}\right) - \frac{\text{Pr}}{\text{Da}}V - \frac{F_C\sqrt{U^2 + V^2}}{\sqrt{\text{Da}}}V$$
$$+ \ \frac{\text{Ra}_m}{\text{Da}}\text{Pr}\,\theta \qquad (7)$$

$$\frac{\partial \theta}{\partial \tau} + \left(U\frac{\partial \theta}{\partial X} + V\frac{\partial \theta}{\partial Y}\right) = \left(\frac{\partial^2 \theta}{\partial X^2} + \frac{\partial^2 \theta}{\partial Y^2}\right) \qquad (8)$$

In equations (6) and (7), ε is the porosity which is assumed uniform throughout the cavity. F_C is the Forchheimer coefficient and given by:

$$F_C = \frac{1.75}{\sqrt{150}}\varepsilon^{-3/2} \qquad (9)$$

The boundary conditions of the governing equations (5)-(8) are set on the basis of physical conditions of the problem described in Figure 1 in the following ways. When non-dimensional time $\tau < 0$, the flow-field variables and their corresponding boundary conditions are set to 0. However for $\tau \geq 0$, initial conditions are taken as 0 and the boundary conditions are given by:

- Zero velocity at all the walls (at $X = 0, 1$ and $Y = 0, 1$) is set by $U = V = 0$.
- Isothermal temperature on the sidewalls (at $X = 0$ and 1) is set by $\theta = 0$.
- Adiabatic condition at $Y = 1$ for the top wall is set by $\partial\theta/\partial Y = 0$.
- Sinusoidal temperature along the bottom wall is set by $\theta = 1 + I\sin(2\pi fX \pm \phi)$, where, I stands for the dimensionless amplitude $[I = A/(T_m - T_c)]$. In this work, I varies from 0.1 to 1, $f = 1 - 5$ and $\phi = \pm 90°$.

A well-established in-house CFD code (Datta *et al.*, 2016; Mahapatra *et al.*, 2015) is used to solve the governing equations and their boundary conditions. The code is based on finite-volume method (FVM) (Versteeg and Malalasekera, 1995), and SIMPLE algorithm (Patankar, 1980). The solution is performed iteratively using under-relaxations for pressure

correction, velocity and temperature equations as 1.0, 0.4 and 1.0, respectively. The solution convergence is obtained by the criteria of maximum residuals below 10^{-8} and maximum mass-defect (of continuity equation) below 10^{-10}. The same code has been repeatedly validated for different problems under natural as well as mixed convection in our earlier works (Datta *et al.*, 2016; Mahapatra *et al.*, 2015; Biswas *et al.*, 2018, 2016a, 2016b, 2016c).

After overcoming initial transience of simulation, all the solutions finally reach steady state (for the study range of parameters). As such, only the steady-state results are considered here for the analysis and discussion. The obtained solutions are post-processed in terms of average Nusselt number (Nu), streamlines and heatlines to assess the enhancement in thermal performance of sinusoidally heated cavity. The average Nusselt number measures the rate of heat transfer through cooling or heating surface. It is used here to compute the net heat transfer from the heated bottom wall under both heating conditions (uniform and non-uniform), which is given by:

$$\text{Nu} = \int_0^1 \left(-\frac{\partial \theta}{\partial Y}\bigg|_{Y=0} \right) dX \tag{10}$$

The average Nusselt number (Nu) in equation (10) is actually the integration of local Nusselt number given by $-(\partial \theta / \partial Y)$ at the bottom ($Y = 0$) of the cavity for $X = 0$ to 1. For the steady-state solutions, the transport of thermal energy flow from hot bottom to either sides of the cavity is analyzed by heatlines. The heatlines are generated from the heatfunction (Π) (Kimura and Bejan, 1983), which is derived from the steady-state energy balance. The heatfunction for the present problem is given as:

$$-\frac{\partial \Pi}{\partial X} = V\theta - \frac{\partial \theta}{\partial Y} \text{ and } \frac{\partial \Pi}{\partial Y} = U\theta - \frac{\partial \theta}{\partial X} \tag{11}$$

The boundary conditions for equation (11) (at right-hand side) are computed from zero wall-velocity condition, and Dirichlet and Neumann temperature conditions. The normal gradients of temperature are zero at top wall (as it adiabatic) and non-zero at bottom and sidewalls (as temperature prescribed). Thus, X and Y gradients of heatfunction Π become zero or non-zero along the boundary walls. It will result a general solution of Π. To obtain a particular solution of this Neumann condition type heatfunction equation, Π has set to 0 as reference at the mid-point of the bottom wall ($X = 0.5$, $Y = 0$) expecting a symmetrical heat transport to either halves of the cavity. This reference value has no impact on the computation of heat transfer, which is based on overall difference of heatfunction. More details about the heatlines visualization can be found in the review of heatlines visualization technique by Mahapatra *et al.* (2018). The streamfunction (ψ) is also computed for visualizing streamlines (that simulate the flow structure) and expressed as:

$$-\frac{\partial \psi}{\partial X} = V \text{ and } \frac{\partial \psi}{\partial Y} = U \tag{12}$$

ψ on all enclosure-walls becomes zero as it is a closed cavity and no external flow enters into it. An integration method is adopted for both the heatfunction and streamfunction equations. However, the integration process is carried out iteratively from all four sides of the cavity until the maximum error reduces to 10^{-8}. A code validation study on the

heatfunction and streamfunction equations is recently presented for a differentially heated cavity in Datta *et al*. (2016).

3. Verification of numerical results

3.1 Code validation

The present in-house code has been tested rigorously under different flow situations (covering all forced convection, natural convection and mixed convection). These results are already reported in many works of us, both numerically and experimentally. For illustrations, in Mahapatra *et al*. (2013) presents the code validation against the famous benchmark solution of de Vahl Davis (1983) on natural convection in differentially heated cavity in terms of stream function, average Nusselt number, and maximum velocities. Latter, Datta *et al*. (2016) have published another code validation against the results of Lauriat and Prasad (1989) for natural convection in a porous enclosure using average Nusselt number. The code validation in terms of average Nusselt number is depicted graphically for a range of flow parameters in Biswas *et al*. (2016a, 2016b, 2016c) for mixed convection in a grooved channel. Furthermore, the validation results for side open cavity under the buoyant flow is also included in Biswas *et al*. (2016a, 2016b, 2016c). For forced convection, the experimental validations of dimensionless pressure drop for blood flow through stenosed coronary artery and leakage flow at different spool displacements for a spool valve, are illustrated by Mandal *et al*. (2010) and Mondal *et al*. (2014), respectively. Moreover, the validation of the present CFD code against our experimental results on natural convection in enclosure is presented in Biswas *et al*. (2016a, 2016b, 2016c).

However, in the present context of multi-frequency bottom heating, a validation problem is chosen from the literature covering all major features of the present problem such as sinusoidal bottom heating, porous medium, heatlines and natural convection in the cavity. The validation study is conducted using a porous square cavity with adiabatic top, non-uniform heating at bottom and both sidewalls as reported in Ramakrishna *et al*. (2013). This work is carried out on natural convection in a porous cavity with thermal boundary conditions using heatlines. In this reference, the non-dimensional temperatures of the bottom-wall and the sidewalls are defined by $\theta = A_T + (1 - A_T) \sin \pi X$ and $\theta = (1 - A_T)Y$, respectively, where A_T is the thermal aspect ratio. The results corresponding to Prandtl number Pr = 0.7, Rayleigh number Ra = 10^5, Darcy number Da = 10 and $A_T = 0.5$ [as reported in Figure 6(b) of Ramakrishna *et al*. (2013)] are presented in Figure 2(a) with the corresponding results obtained from the present code. Through the comparison of streamlines, isotherms and heatlines of the present predictions with the respective plots of the published results (Ramakrishna *et al*., 2013), it is understandable that the contour plots of both the results match well. So, it can be inferred here that the implementation of all CFD artifacts (such as grid distribution, differencing scheme, convergence setting, boundary conditions including the non-uniform distributions of temperatures in different walls) and the post-processing of data (particularly for the solutions of streamlines and heatlines) are reliable, and the accuracy and performance of the present code is satisfactory.

3.2 Grid independence study

For the generation of grid independent solution, extensive grid testing is conducted using six different grid sizes ($100 \times 100, 200 \times 100, 400 \times 100, 450 \times 150, 500 \times 150$ and 550×200) considering non-uniform heating [$\theta = 1 + I \sin(2\pi fX + \phi)$] at the bottom wall and Da = 10^{-4} and $\varepsilon = 0.6, I = 1, f = 1, 5$ and a range of Ra_m values ($1 - 10^4$). The grids are distributed uniformly along the horizontal direction and non-uniformly along the vertical direction. Along the horizontal direction finer grid-size is provided (using 400, 500, 550 grids) to
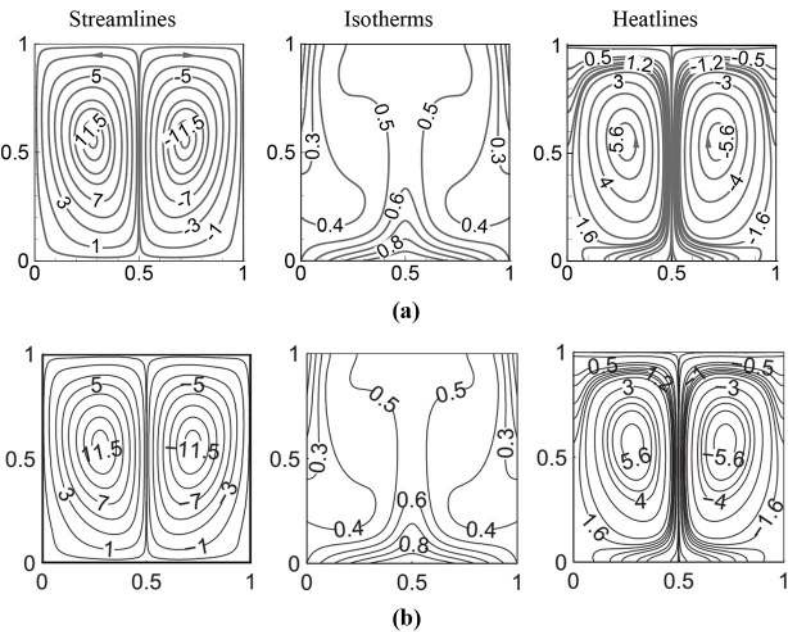
Figure 2.
Code validation at
Pr = 0.7, Ra = 10^5,
Da = 10 and A_T = 0.5

Notes: (a) The present predictions in top row; (b) the published results of
(Ramakrishna *et al*. 2013) in bottom row

capture multi-cellular flow vortices near the sinusoidally heated bottom wall. Whereas, along the vertical direction with grid sizes of 150 and 200, the finest grid of 0.0001 is taken at bottom. The grid results are prepared in Table II using average Nu of sinusoidally heated wall (at Y = 0) for both low and high frequencies of heating (f = 1, 5). Except the first grid size (100 × 100), both Nu values and relative errors (with respect to previous lower grid size shown in the brackets) are indicated in Table II. After analyzing data, it is clear that, for 500 × 150 grid size, the error is found < 1.4 per cent and it is acceptable. So, 500 × 150 is most suitable for simulating the present case of multi-frequency heating. The grid size in the

			Nu (% error with respect to immediate coarser grid)				
Frequency	Ra_m	100 × 100	200 × 100	400 × 100	450 × 150	500 × 150	550 × 200
f = 1	10^0	13.904	15.658 (11.20)	17.404 (10.03)	17.771 (2.07)	18.038 (1.48)	18.106 (0.37)
	10^1	13.918	15.668 (11.17)	17.412 (10.02)	17.774 (2.04)	18.041 (1.48)	18.107 (0.37)
	10^2	14.610	16.338 (10.58)	18.072 (9.60)	18.387 (1.71)	18.652 (1.43)	18.711 (0.31)
	10^3	20.523	22.280 (7.89)	24.030 (7.28)	24.307 (1.14)	24.574 (1.09)	24.732 (0.64)
	10^4	31.571	33.571 (5.96)	35.391 (5.14)	35.571 (0.51)	35.744 (0.48)	35.894 (0.42)
f = 5	10^0	18.785	20.568 (8.67)	22.332 (7.90)	22.734 (1.77)	23.001 (1.16)	23.270 (1.16)
	10^1	18.841	20.603 (8.55)	22.362 (7.87)	22.759 (1.75)	23.026 (1.16)	23.293 (1.15)
	10^2	20.661	22.377 (7.67)	24.095 (7.13)	24.442 (1.42)	24.706 (1.07)	24.969 (1.06)
	10^3	28.966	30.734 (5.75)	32.459 (5.31)	32.649 (0.58)	32.912 (0.80)	33.179 (0.81)
	10^4	43.140	44.612 (3.30)	46.301 (3.65)	46.263 (0.08)	46.521 (0.55)	46.783 (0.56)

Table II.
Grid independence
study using Da =
10^{-4}, ε = 0.6, I = 1,
f = 1, 5 and ϕ = 90°

horizontal direction is required very high to properly capture multi-frequency temperature variation along the bottom wall and the associated flow-physics.
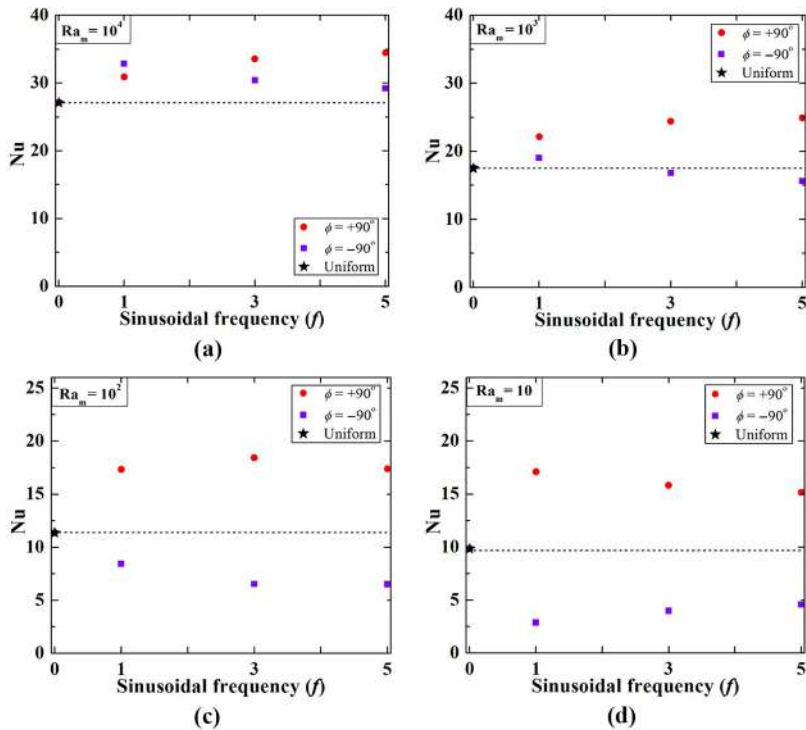
4. Results and discussion
Towards the heat transfer enhancement, the efficacy of sinusoidal heating, particularly at higher spatial frequency is investigated here. The enhancement in heat transfer will provide better thermal performance or size reduction of a system; moreover, it can compensate the reduction in heat transfer when the porous substance is necessarily present in a system. Keeping all these facts in mind, the present study on a porous cavity is conducted exhaustively applying non-uniform sinusoidal heating. The sinusoidal form is considered here to fulfill the mean-temperature constraint of heating. This mean-temperature can right way compare the outcomes under different heating frequencies. The uniform heating configuration is also simulated to obtain the reference data for the comparison. Both the heating results (uniform and sinusoidal) are demonstrated collectively with the help of graphical illustrations of parametric variations considering Darcy–Rayleigh number $Ra_m = 1, 10, 10^2, 10^3, 10^4$, Darcy number $Da = 10^{-4}$ and porosity $\varepsilon = 0.6$. For sinusoidal heating, the amplitude varies through parameter I as 0.1, 0.3, 0.5, 0.8 and 1. The frequency of sinusoidal heating is varied as $f = 1, 3$ and 5. The phase deviation angle is varied as $\phi = \pm 90°$. It is to be noted here that the numerical simulation is executed using the transient form of the governing equations and any oscillating behavior of global parameters/flow-variables is not observed at longer simulation time. It indicates the final solutions as steady-state solutions. Considering the practical applicability, the final steady-state results are discussed in this work.

To focus the individual aspects of the problem, this section is constructed in six more sub-sections. First of all, in Section 4.1, the overview of heat transfer characteristics under multi-frequency heating at different values of Ra_m and phase angles is presented to understand the impact of multi-frequency heating. To go deep into the multi-frequency behavior, single frequency behavior in relations to uniform heating and the variations in phase-angle and amplitude is explored. Accordingly, the impact of uniform and non-uniform heating (considering phase angles) is illustrated in the form of comparison in Section 4.2. Next in Section 4.3, heat flow-dynamics at amplitude variation is discussed. Heat flow-dynamics at multi-frequency is elaborated in Section 4.4. The section 4.5 is prepared for the understanding of boundary layer flow over the sinusoidal-heating bottom and corresponding boundary layer thicknesses at $f = 3$. Finally, the analysis of heat transfer enhancement is reported in Section 4.6 considering different parametric variations.

4.1 Overview of heat transfer characteristics with multi-frequency sinusoidal heating
The essence of the present investigation on multi-frequency sinusoidal heating at the bottom of the porous cavity is presented in Figure 3 with $I = 1$, $Da = 10^{-4}$ and $\varepsilon = 0.6$. It describes the heat transfer characteristics of the present problem under (spatial) multi-frequency heating following the sinusoidal profile of temperature as described in Figure 1(b) for different Darcy–Rayleigh numbers (Ra_m). In Figure 3(a) at $Ra_m = 10^4$, with the increase in frequency of heating (from $f = 1$ to 3, then 5), consistent increase in Nu (or heat transfer) is observed for the phase angles ($+90°$ and $-90°$) of sinusoidal heating. However, their trends are opposite (rising for $+90°$ and falling for $-90°$) as the frequency increases from 1 to 5. With positive phase angle ($\phi = +90°$), the heat transfer is substantially enhanced. The average Nusselt number for uniform heating (as having a single value, shown by '*' on the vertical axis of the figures) is drawn by a dotted horizontal straight line as a reference to visually reflect the rise in Nu under different values of f, ϕ and Ra_m. The thermo-fluid flow
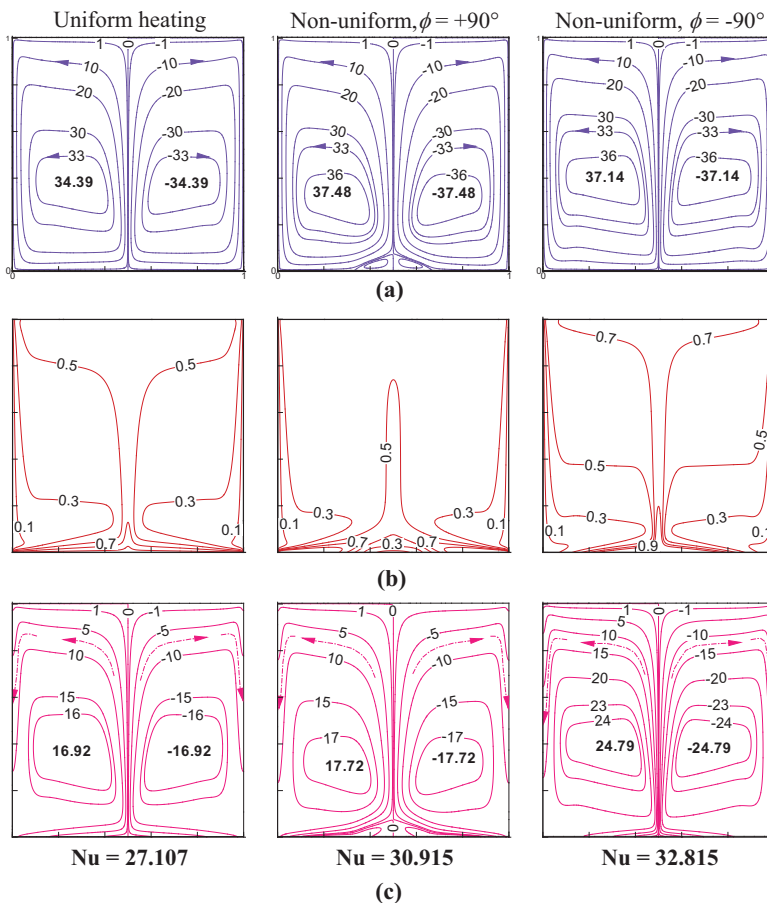
Figure 3.
Heat transfer
characteristics for
multi-frequency
bottom-heated porous
cavity at Da = 10^4,
ε = 0.6, I =1

Notes: (a) Ra$_m$ = 10^4; (b) Ra$_m$ = 10^3; (c) Ra$_m$ = 10^2; (d) Ra$_m$ = 10

dynamics of the working fluid in the cavity is governed by both conduction and convection modes of heat transfer. Evidently, heat transfer is found to be maximum at the highest value of Darcy–Rayleigh number, Ra$_m$ = 10^4, because of buoyancy-induced stronger flow-velocity. As Ra$_m$ decreases, Nu values for all the cases (uniform, ϕ = +90° and ϕ = −90°) in Figure 3(c) and 3(d) reduce with the reduction in convective strength and flow-velocity. However, the heat transfer enhancement for the positive phase angle (ϕ = +90°) is found higher for all the frequencies. In contrast, for the negative phase angle (ϕ = −90°) at Ra$_m$ ≤ 10^3 shows negative impact on the heat transfer irrespective of the value of frequency. At Ra$_m$ = 10^3 [in Figure 3(b)], heat transfer of ϕ = −90° is very close to that of uniform frequency. Furthermore, at further lower values of Ra$_m$ (≤ 10^2), the trends of heat transfer of ϕ = +90° and ϕ = −90° get reversed. It is prominently observed by comparing Figure 3(a) (Ra$_m$ = 10^4) with Figure 3(d) (Ra$_m$ = 10). It is because of the fact that at lower Ra$_m$, thermal conduction dominates over thermal convection. It reverses at higher Ra$_m$. From the application point of view, to exercise significant convective heat transfer, the value of Ra$_m$ should be higher. The findings from Figure 3(a) at Ra$_m$ =10^4 suggest that, Nu persistently increases with the increment of frequency of sinusoidal heating irrespective of phase angles. Though this trend demands more results at further high frequencies, the same is not persuaded here considering the limitation in practical implementation. The reasons behind of all these trends of heat transfer enhancement/characteristics can be realized by close examining the different flow fields. This exercise is taken up systematically in the following sections.

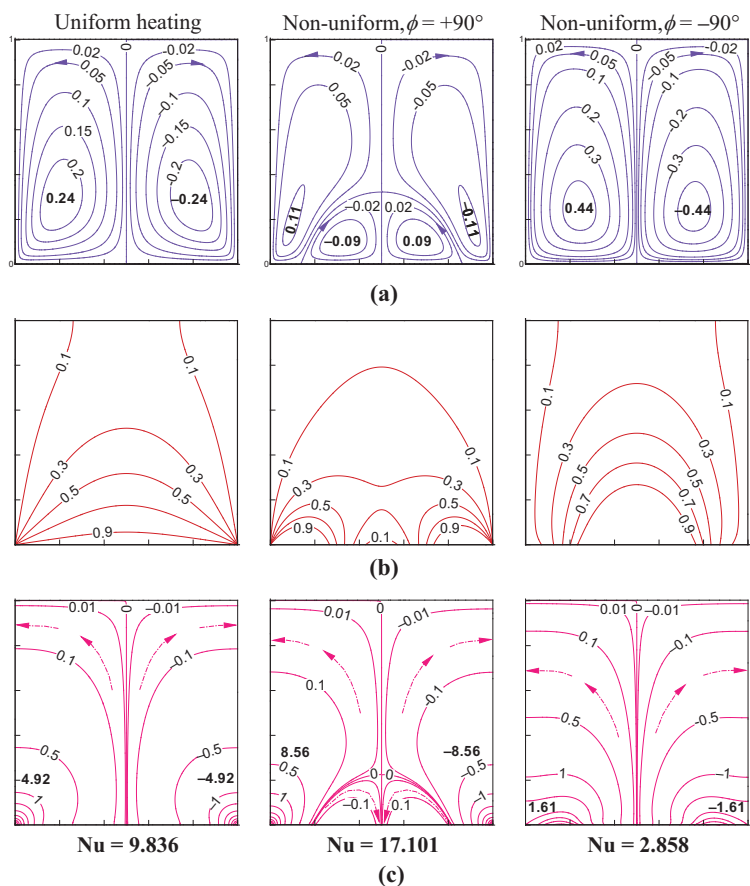*4.2 Impact of uniform heating and non-uniform heating at f = 1*
The fluid-flow field and the temperature field under uniform and sinusoidal heating are presented in Figures 4 and 5 considering particular flow-conditions at $f = 1$ and $Ra_m = 10^4$ and 10. Both the figures consist of streamlines in the top row, isotherms in the middle row and heatlines in the bottom row. In general, because of bottom heating, the heated fluid from the bottom region moves upward through the middle portion of the cavity. The flow continues from upper region of the cavity in downward direction following the cold sidewalls. Thus, two counter-rotating primary circulations are developed in the plots of streamlines and heatlines. The contour plots of all flow fields (indicated by streamlines, isotherms and heatlines) become symmetrical in either vertical halves of the cavity, as the imposed thermal boundary conditions are symmetric. In this problem (Figure 1), both sidewalls are cold, top wall is adiabatic, and bottom wall from its mid-point is symmetrically heated. As a result of these thermal conditions, thermal energy from the bottom-wall (which

Notes: (a) Streamlines; (b) isotherms; (c) heatlines

Figure 4.
Impact of uniform
and sinusoidal
heating at single
frequency for Da =
10^{-4}, $\varepsilon = 0.6$, $I = 1$
and $Ra_m = 10^4$

Uniform heating   Non-uniform, $\phi = +90°$ Non-uniform, $\phi = -90°$

(a)

(b)

Nu = 9.836   Nu = 17.101   Nu = 2.858

(c)

Notes: (a) Streamlines; (b) isotherms; (c) heatlines

acts as heat source) flows to the sidewalls (which acts as heat sink) through certain well-defined corridors formed by heatlines. Any two successive heatlines with their ends on the bottom and sidewalls construct the pathway for fixed amount energy transport from the source to the sink. Along the corridors, the local intensity of total heat flux varies depending upon the widths of the individual corridors. The width of energy corridors becomes narrowed when convective heat flux is very strong. The intensified distribution of heatlines near the hot wall (at bottom and bottom-middle regions of the cavity) indicates the high magnitude energy flow through the narrowed flow section, which finally spreads over the entire lengths of the sidewalls. The inactive energy-flow areas of the cavity are filled with energy recirculation cells as like circulation vortices in the streamline plots. In case of these energy and mass vortices (or circulations), the negative ('-') sign before the contour values indicates clockwise (CW) rotation, whereas, the positive ('+') sign means counter-clockwise (CCW) rotation.

*4.3 Heat flow-dynamics under sinusoidal heating (variable amplitude at f = 1)*
The dynamics of heat-fluid flow under sinusoidal heating can better be realized by studying the stretch between uniform heating and non-uniform heating in steps from small amplitude to large amplitude. Corresponding studies on amplitude variation of sinusoidal heating are shown in Figures 6 and 7. For it, three different values of dimensionless amplitudes (I) are chosen as 0.05 (close to uniform heating), 0.5 and 1 for both positive (Figure 6) and negative (Figure 7) phase angles ($\phi = \pm 90°$) at $f = 1$ and $Ra_m = 10^3$. In these figures, the heatlines are drawn at top and the imposed temperature profile is indicated below the streamline-isotherm combined plot at bottom. The temperature profile of fluid at the nearest nodes of the bottom wall (which is located at a distance of 0.0001 from it) is also shown in the temperature profile panel of the figure. Evidently, these two profile curves are very close to each other. Under the steady state condition of simulation, the fluid temperature near the hot wall becomes almost same as the temperature of the applied condition. In general, the temperature of fluid layer immediate to wall node changes following the heating condition.
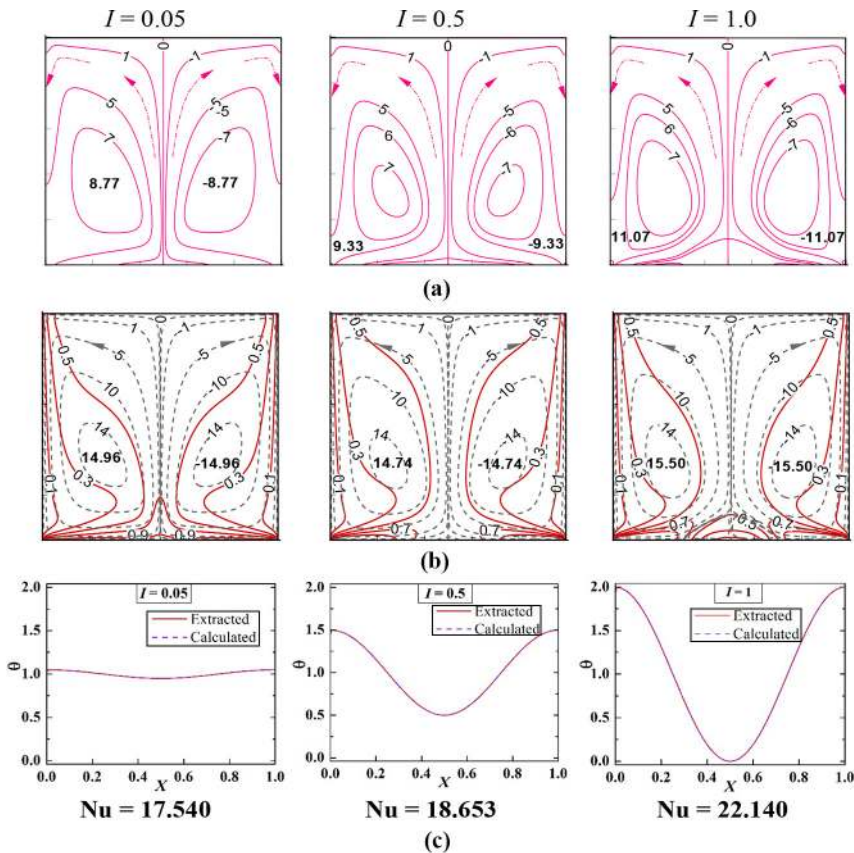
Figure 6.
Impact of amplitude variation of sinusoidal heating at $Ra_m = 10^3, Da = 10^{-4}$, $\varepsilon = 0.6, f = 1, \phi = +90°$

Notes: (a) Heatlines; (b) combined isotherms-streamlines (dotted lines for streamlines); (c) bottom-wall temperature profiles
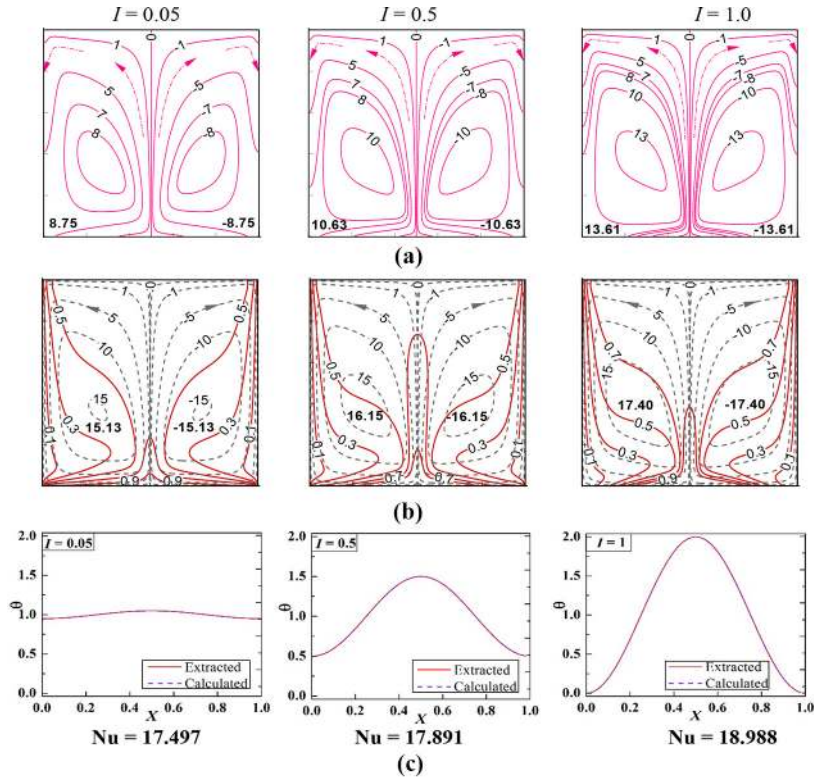
Figure 7.
Impact of amplitude
variation of
sinusoidal heating at
$Ra_m = 10^3, Da = 10^{-4},$
$\varepsilon = 0.6, f = 1, \phi =$
$-90°$

Notes: (a) Heatlines; (b) combined isotherms-streamlines (dotted lines for
streamlines); (c) bottom-wall temperature profiles

However, a sharp fall in the fluid temperature at $X = 0$ and 1 for positive phase angle
(Figure 6) is attributed from the interaction of fluid with the adjacent vertical cold sidewalls.
It is should be mentioned here that, for all amplitude values, the area under the temperature
profile curve is same, it results into the mean-temperature same irrespective of various
frequencies of the sinusoidal heating. Using this mean-temperature constraint of heating
(which under a lumped modeling could be an index of heat load), the present work is
conducted.

The inherent effect of amplitude variation (of temperature) can be realized from
the streamlines, isotherms and heatlines as shown in Figure 6 for $\phi = +90°$ and
Figure 7 for $\phi = -90°$. At very low amplitude, $I = 0.05$ (in both Figures 6 and 7), the
sinusoidal temperature profile acting on the bottom wall is very close to uniform heating (θ
≈ 1 at bottom). In this scenario, the flow fields are very close to the flow fields of uniform
heating. However, these flow fields at $Ra_m = 10^3$ strongly differ in strengths in comparison
with the flow-fields of uniform heating shown in Figure 4 (for $Ra_m = 10^4$) and Figure 5 (for
$Ra_m = 10$).

As the amplitude I becomes 0.5, the wall-end temperatures (θ) increase to 1.5 and the
middle temperature falls to 0.5 as indicated in temperature distribution panel of Figure 6 for

$\phi = +90°$. However, for negative phase angle ($\phi = -90°$) in Figure 7 with amplitude $I = 0.5$, the wall-end temperatures (θ) decrease to 0.5 and the middle temperature rises to 1.5. For both the cases of ϕ, the change in patterns of all flow-field distributions in the cavity is found insignificant except a small-localized change near the middle of the bottom wall. In Figure 6 (for $\phi = +90°$) a small vortex is formed. The flow-structures remain symmetric. The impact on maximum Π or ψ is also small ($\psi_{max} = 14.734$ and $\Pi_{max} = 9.326$). However, in Figure 7 (for $\phi = -90°$), because of an increase in middle temperature ($\theta = 1.5$), the prominent peaks on isotherm curves are formed. It results the increased fluid and energy circulations as noted by $\psi_{max} = 16.148$ and $\Pi_{max} = 10.603$.

At the sinusoidal amplitude $I = 1.0$, the afore-mentioned observations are markedly magnified. For $\phi = +90°$ (in Figure 6), the vortex adjacent to the bottom wall grows to a prominent shape. This secondary vortex develops from the local temperature variation along the bottom wall. In between the primary vortex and secondary vortex, some isotherms peaks are formed surrounding the secondary vortex. The changes in maximum values of Π and ψ (with respect to uniform or $I = 0.05$) are noticeable. However, for $\phi = -90°$ (in Figure 7), except the monotonous growth, all the flow patterns are remained unaltered. With the Darcy–Rayleigh number $Ra_m = 10^3$, magnitude of quantitative heat transfer enhancement of the positive ϕ case (compared to uniform heating) is about 0.16, 6.52 and 26.43 per cent for $I = 0.05$, 0.5 and 1, respectively. For the negative ϕ case, it is about 0, 2.17 and 8.43 per cent for $I = 0.05$, 0.5 and 1, respectively. However, it should be noted here that the order of enhancement strongly depends on Ra_m values (as indicated earlier in Figure 3).

Further to the above-mentioned analysis, the details of transport phenomena occurring at the heated bottom wall in lower region of the cavity (owing to amplitude variation at $f = 1$) is closely examined using Figures 8 and 9 respectively for $\phi = +90°$ and $\phi = -90°$. The part (a) of these figures is magnified views of the bottom regions of Figures 6 and 7 (heatlines in top panel, combined streamlines-isotherms in bottom panel); and the part (b) of these figures is the distribution of local Nusselt number. The imposed temperature variation in terms of different sinusoidal amplitude severely affects the rate of local heat transfer as indicated by local Nu in Figures 8(b) and 9(b). As I from 0.05 increases, the temperature of the bottom wall significantly changes with X. It greatly influences the fluid temperature in the lower region of the cavity. As I increases in Figure 8(a), from single isothermal peak, multiple peaks (2 peaks for $I = 0.5$ and 3 peaks for $I = 1$) are formed. It results in the variation of local Nusselt number along X in Figure 8(b). From it, one interesting fact reveals that local Nu can be both positive and negative, that is, with the strong temperature variation (with $I = 1$) both heating and cooling take place through the bottom wall. However, with the negative phase angle ($\phi = -90°$) in Figure 9(a), the middle single isothermal peak becomes gradually strong with I. It significantly alters the pattern of local Nu in Figure 9(b). Though the variation in local Nu along X persists, in contrast to earlier $\phi = +90°$ case, only heating is done through the bottom wall continually (for all values of I).

### 4.4 Heat flow-dynamics under multi-frequency sinusoidal heating
The dynamics of heat-fluid flow under multi-frequency sinusoidal heating is explained with the help of Figures 10 and 11, respectively for positive and negative phase angles using $Ra_m = 10^3$. The overall structure of flow-fields except the bottom region is similar to those observed earlier with frequency $f = 1$ in Figures 6 and 7. The (twin) primary circulations in the heatlines plots (top rows) and streamlines plots (middle rows) are found to persist irrespective of any spatial frequencies or phase angles. The values of circulations are marginally sensitive at higher spatial frequencies $f = 3$ and 5. However, a complex flow structure near the bottom wall is observed with the increase in frequency of sinusoidal
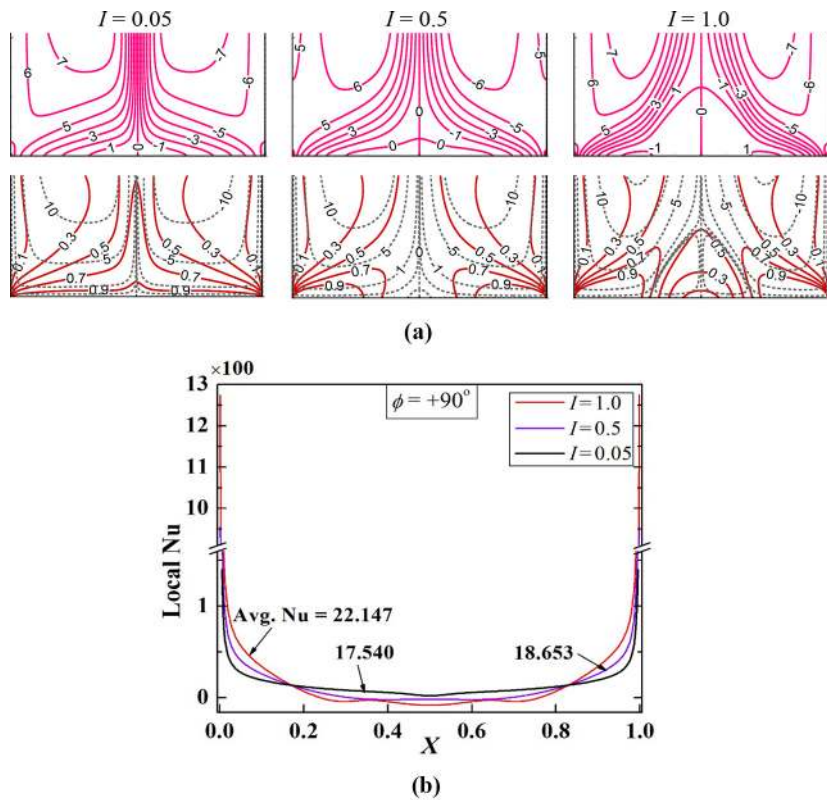
Figure 8.
Heat transport
phenomena near the
bottom wall at $Ra_m = 10^3$, $Da = 10^{-4}$, $\varepsilon = 0.6$, $f = 1$, $\phi = +90°$

Notes: (a) Enlarged view from Figure 6 consisting of heatlines and combined
streamlines-isotherms (dotted lines for streamlines); (b) local Nusselt number along
the bottom wall

heating. A numbers of tiny energy and mass vortices are formed because of the higher
frequency (above $f = 1$). The number of vortices is a function of frequency of heating.

The analysis of frequency variation is further continued with the detailed blow-up view
of the bottom region of the cavity in Figure 12 in terms of heatlines followed by streamlines
and isotherms (in the successive rows). Figure 12 clearly displays these vortices for the
positive phase angle ($\phi = +90°$) in Figure 12(a), the negative phase angle ($\phi = -90°$) in
Figure 12(b). Phase angle based comparison of local Nu distribution along the bottom wall is
examined in Figure 12(c). As the imposed temperature is varied sinusoidally, local Nu
follows the same pattern of variation along the bottom wall of the cavity. Spatially along the
length of bottom wall, both heating and cooling take place sinusoidally at $f = 3$ and 5 in
alternate manner. For the negative phase angle, the number of intermediate heating zones is
same as the frequency of sinusoidal heating. Whereas, for the positive phase angle, the
number of intermediate cooling zones is same as the frequency. At the extreme values of X
(at sidewalls), the shooting rise of local Nu is noted for $\phi = +90°$. It happens so because of
large temperature difference with the cold sidewalls. This feature at the ends of the bottom
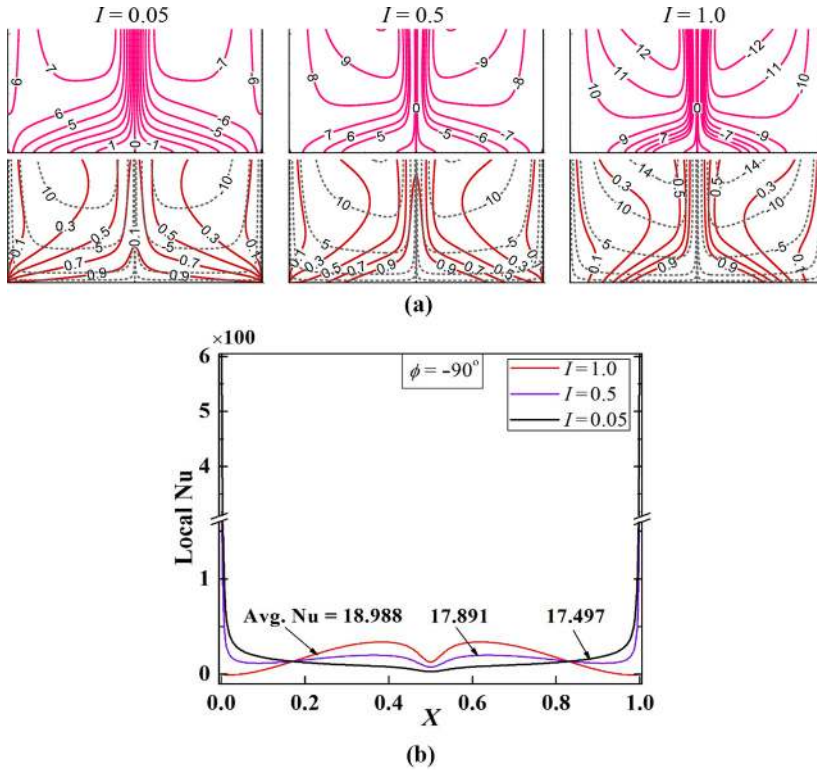
Notes: (a) Enlarged view from Figure 7 consisting of heatlines and combined
streamlines-isotherms (dotted lines for streamlines); (b) local Nusselt number along
the bottom wall

wall is totally absent for ϕ = $-90°$ as the temperature difference there becomes zero; local
Nu thus starts and ends with 0 as shown in Figure 12(c).

The effect of multi-frequency is remarkably prominent at higher Darcy–Rayleigh
number, so it is demonstrated in Figure 13. In fact, the characteristics of heat-flow dynamics
is found more exaggerated at higher Ra_m and higher frequency (as also established earlier in
Figure 3). Comparative assessment is depicted considering uniform heating (i.e. f = 0),
positive phase angle (ϕ = $+90°$) and negative phase angle (ϕ = $-90°$) for each heating
frequency, f = 1, 3 and 5 [in Figure 13(a)-13(c)]. The underneath reason could be realized from
Figure 13 that covers most of the important information about local Nu distribution, average
Nusselt number, identification of heating zones (ZH) and cooling zones (ZC) under varying
frequency (f = 0 − 5) and phase angle. At Ra_m = 10^4 in Figure 13, the oscillation of local Nu
(along X) persistently increases as f increases from 1 to 5. In the figure, the peak values of
local Nu are found consistently higher at higher frequencies. However, the average Nusselt
number surprisingly remains less affected at higher f = 5. The reason behind this fact is the
cancellation of augmented positive heating by the enhanced intermediate cooling (negative
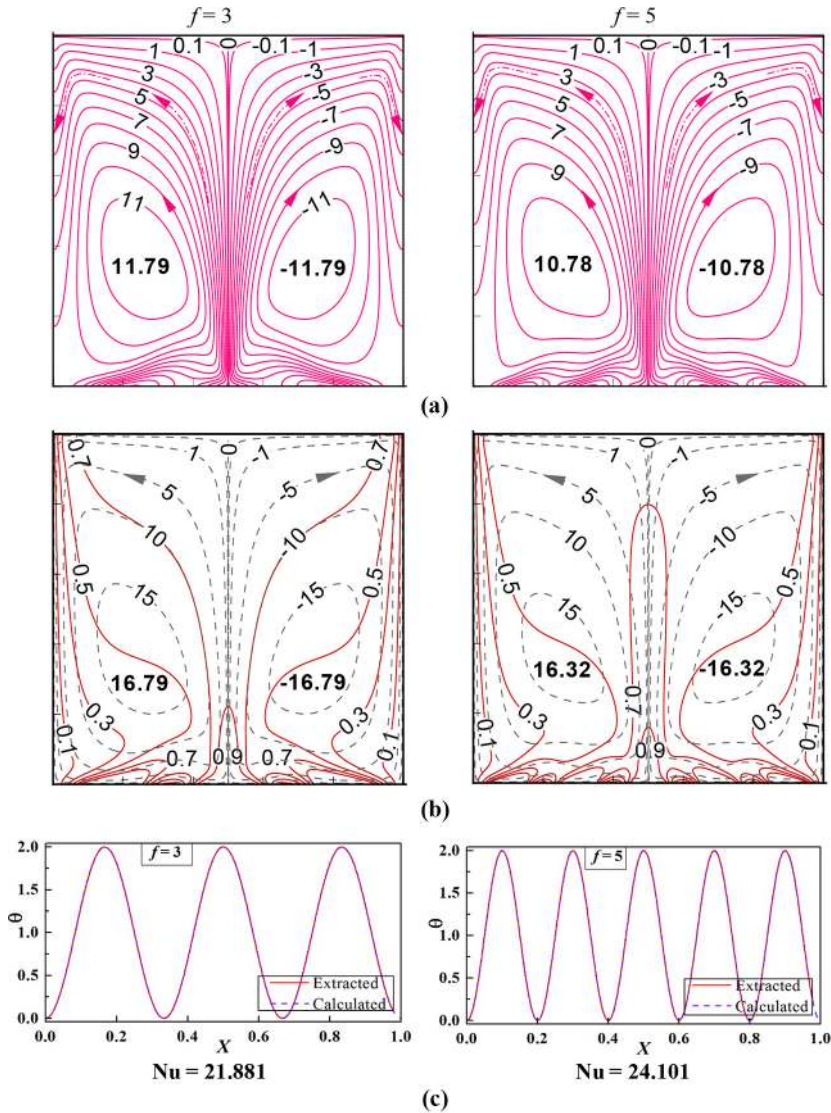heating) that appears periodically.
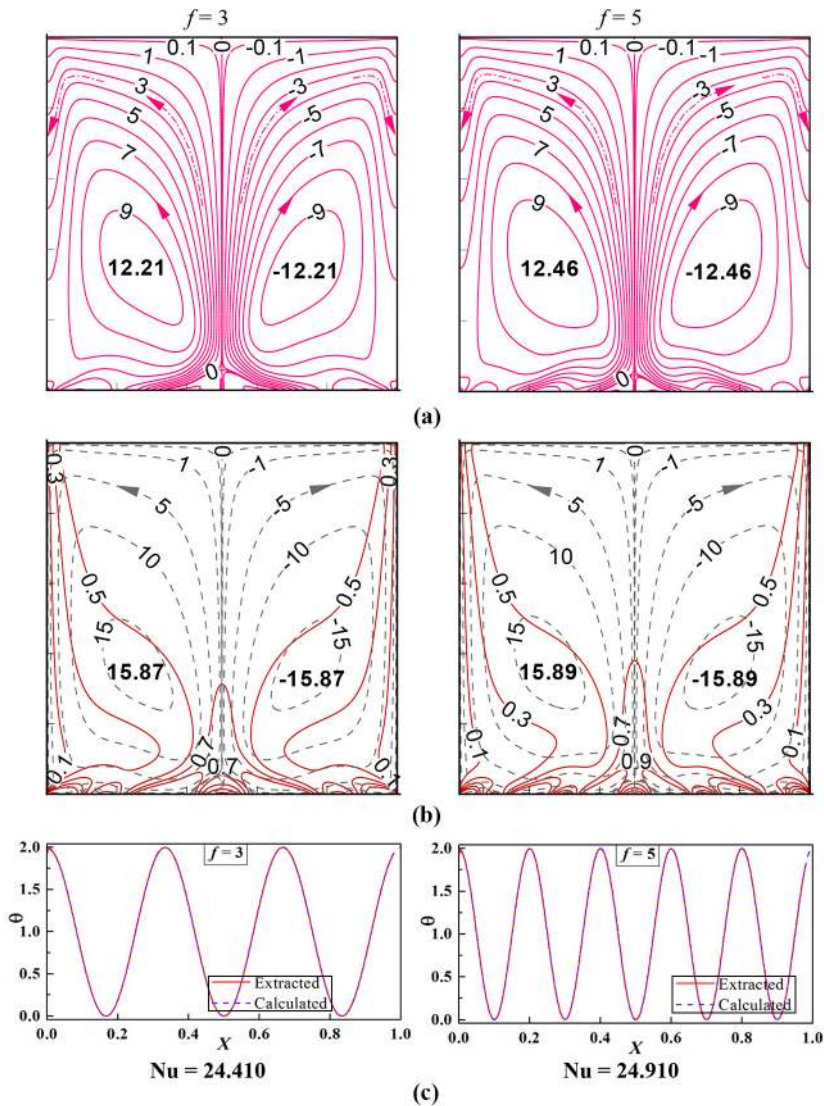
Figure 10.
Impact of multi-
frequency heating
($f = 3, 5$) at $Ra_m = 10^3$,
$Da = 10^{-4}$, $\varepsilon = 0.6$,
$I = 1$, $\phi = 90°$

Notes: (a) Heatlines; (b) combined streamlines-isotherms (dotted lines for
streamlines); (c) bottom-wall temperature profiles

### 4.5 Appreciation of boundary layer flow and thicknesses

For in-depth understanding of heat and fluid flow under multi-frequency heating, the fluid-
flow pattern near the sinusoidally heated bottom wall is investigated taking fixed values of
$Da = 10^{-4}$, $\varepsilon = 0.6$, $I = 1$ for $Ra_m = 10^4$ and 10^3 in Figures 14 and 15, respectively. For the
grasp of the change in flow patterns, the isotherms and velocity vectors under uniform
heating (constant bottom-wall temperature, $f = 0$) is presented first in Figures 14(a) and 15(a).

Figure 11.
Impact of multi-
frequency heating
($f = 3, 5$) at $Ra_m = 10^3$,
$Da = 10^{-4}$, $\varepsilon = 0.6$,
$I = 1$, $\phi = -90°$

Notes: (a) Heatlines; (b) combined streamlines-isotherms (dotted lines for
streamlines); (c) bottom-wall temperature profiles

Thereafter, different frequencies are considered [row-wise in Figures 14(b), 14(c), 15(b) and 15(c)]
for both the phase angles of $\phi = +90°$ [left in Figures 14(b) and 15(b)] and $\phi = -90°$ [right in
Figures 14(c) and 15(c)]. Under the steady uniform heating in Figures 14(a) and 15(a), the
existence of velocity and thermal boundary layers is observed in the stretch of horizontal flow
near the bottom wall. The descending flow along the cold sidewalls, taking 90° turns at the
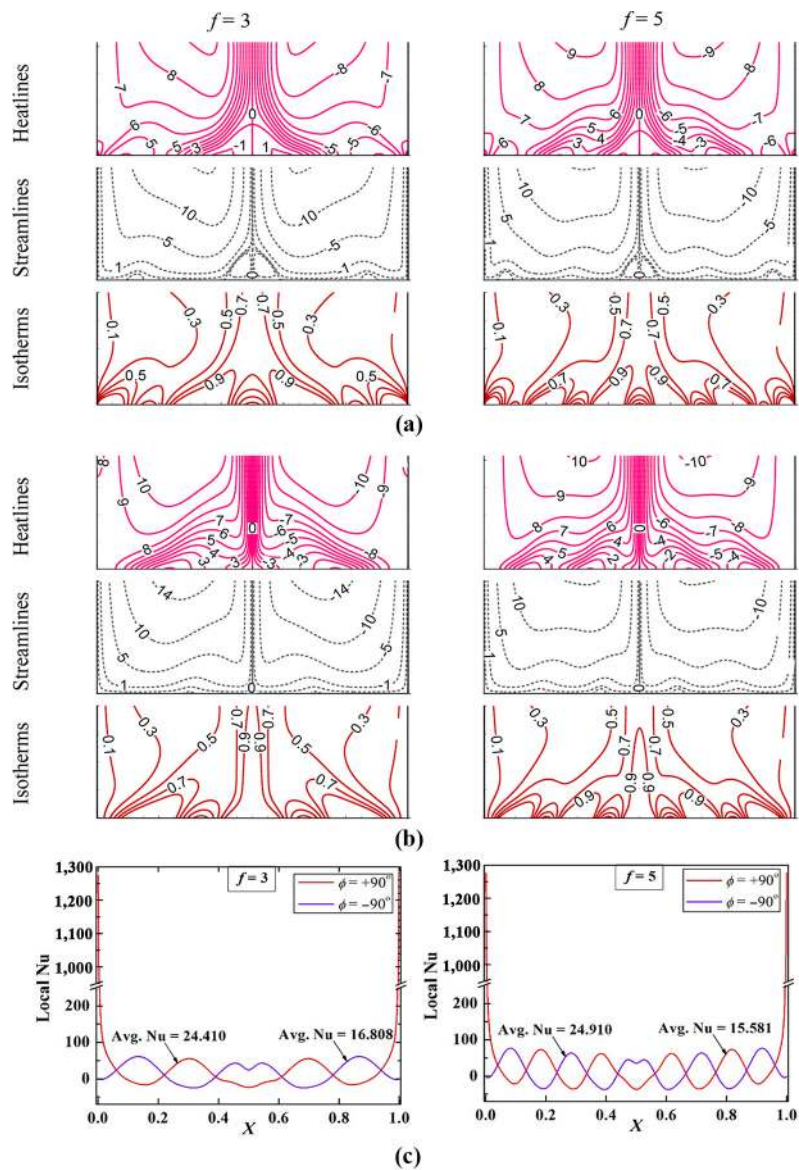
Figure 12.
High frequency heat transport phenomena near the bottom wall at $Ra_m = 10^3$, $Da = 10^{-4}$, $\varepsilon = 0.6$, $I = 1$

Notes: (a) $\phi = +90°$; (b) $\phi = -90°$

bottom corners from both end sides, becomes parallel to the bottom wall and flows up to the middle of the bottom wall. Thereafter, it rises upward like a central plume. The isotherm adjacent to the bottom wall reflects thick boundary layer at the center and relatively thin boundary layer at both ends of bottom wall. Here exist two streams of fluid flow for either halves of the bottom wall. This scenario of temperature distribution and fluid-flow pattern
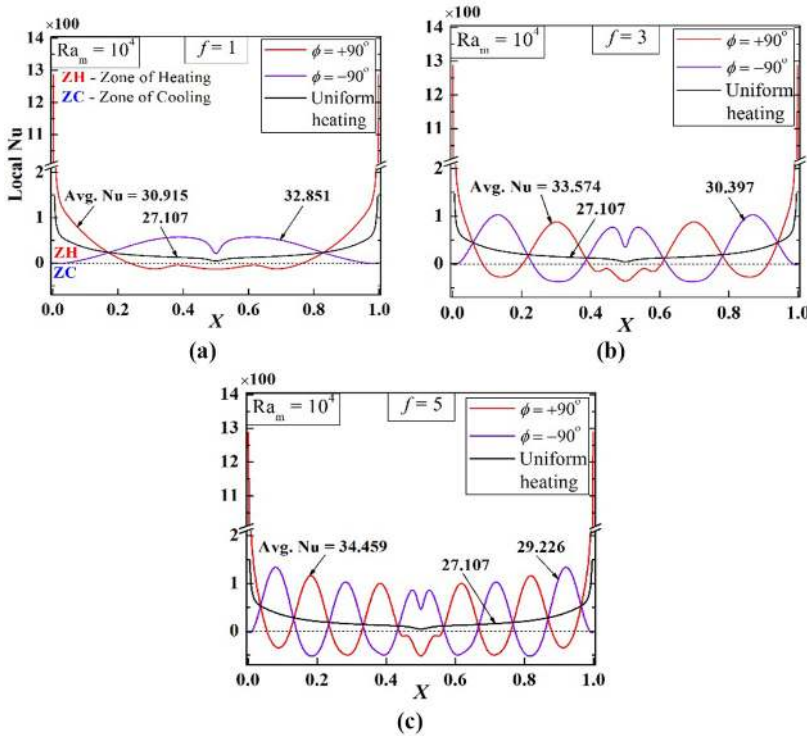
Note: The dotted line is used to demarcate heating and cooling zones (ZH, ZC)

changes severely under the sinusoidal heating along with its different (spatial) frequencies as shown in the part (b) and (c) of Figures 14 and 15. Under the non-uniform sinusoidal heating, the primary circulations (counter-clockwise in the left-half and clockwise in the right-half) remain unaltered along with the single central plume. However, beneath these circulations, the development of wavy boundary layer (and small eddies in some cases) near the bottom wall is observed. It happens in the depression zone of temperature profile (where θ approaching to 0) because of intermittent cooling through the same bottom wall. The descending flow-streams from the sidewalls flow over the sinusoidally heated bottom wall forming small undulation. Given uneven (oscillatory) heating, usual boundary layer flow with monotonous growth (or decay) of boundary thicknesses gets totally disrupted. The pulsatile heating as if leads to partial stripping off the notional boundary layer, in periodical manner. This partial stripping of the boundary layer flow is the main reason behind the enhanced heat transfer (Mahapatra *et al.*, 2015) under sinusoidal heating, although the mean-temperature of heating is always maintained constant. From Figures 14 and 15 with the same reference vector, it is apparent that convective velocity is higher at $Ra_m = 10^4$ and relatively lower at $Ra_m = 10^3$. The effect of phase angle at $f = 1$ on the formation of waviness or eddies is found different for $\phi = +90°$ [Figures 14(b) and 15(b)] where secondary eddies are formed, and for $\phi = -90°$ [Figures 14(c) and 15(c)] where they are absent. With the increase in heating frequency (at higher f values), the undulation (in the flow pattern near the bottom wall) enhances because of the presence of more depression points of temperature.
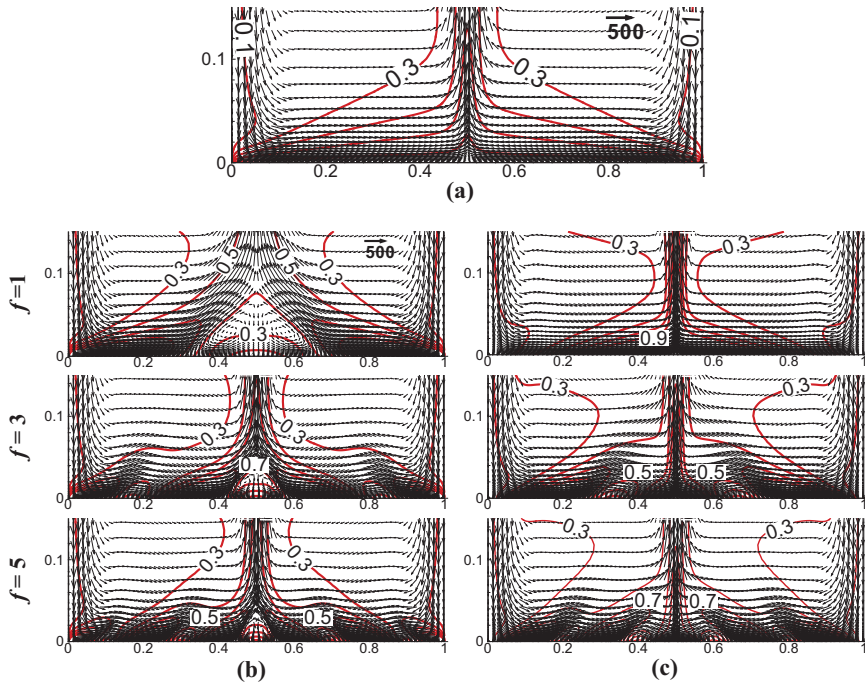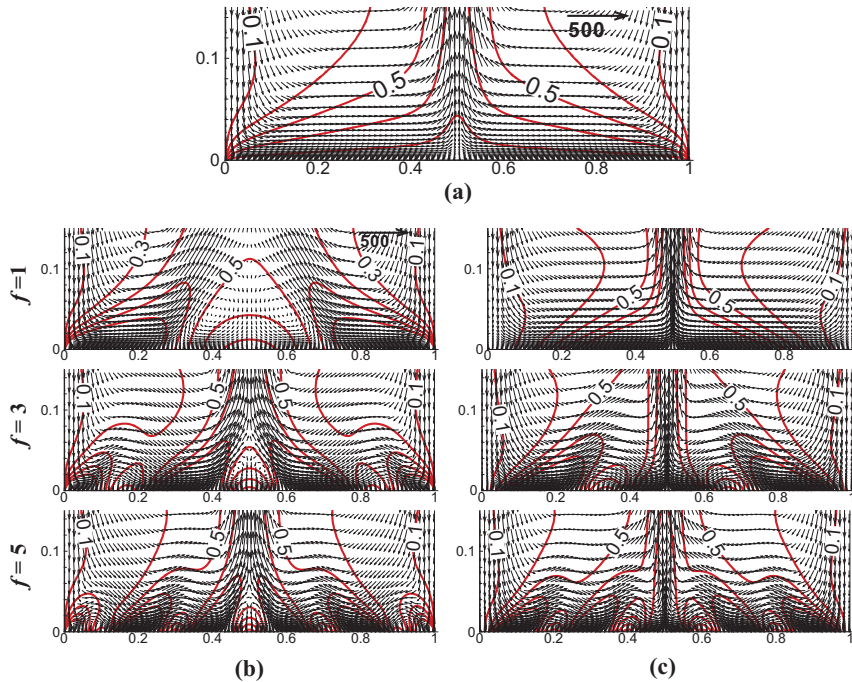
Figure 14.
Appreciation of near-boundary thermo-fluid flow phenomena at $Ra_m = 10^4$, $Da = 10^{-4}$, $\varepsilon = 0.6$ using velocity vectors (shown by arrows) and isotherms (continuous line)

Notes: (a) Uniform heating; (b) sinusoidal heating with $\phi = +90°$; (c) sinusoidal heating with $\phi = -90°$

To get more insight into the thermal and velocity boundary layer thicknesses at the bottom wall, the CFD simulated velocity and temperature profiles near the bottom wall are prepared at the certain sample points ($X_1 = 0.0825$, $X_2 = 0.170$, $X_3 = 0.250$, $X_4 = 0.334$, $X_5 = 0.416$) along the bottom wall. These profiles are presented for different parametric conditions in Figures 16 and 17 along with their blow up views alongside marked as "A" and "B." As the bottom wall is stationary, U velocity increases from zero at wall and reaches a peak value indicated (by a dot marker). With the notional concept of boundary layer flow, these peak points could be assumed as a tentative estimate of velocity boundary layer thickness. In similar way, the peak points on the temperature curves are marked. These data are used for the construction of tentative boundary layer thicknesses presented in Figure 18 and discussed in the next paragraph.

In Figure 18, the appreciation of boundary layer thicknesses (δ_v, δ_t) extracted from the computed flow-fields by CFD, is taken up considering all the heating configurations (uniform heating, positive and negative phase angles) collectively. Only the left half of the bottom region (excluding the zones of descending flow along the sidewalls and the central plume) is addressed here as the flow structure is symmetric about the mid-vertical plane. The trends of the thickness curves for thermal boundary layer [Figure 18(a)] and velocity boundary layer [Figure 18(b)], are drawn on the basis of some sample points ($X_1 = 0.0825$, $X_2 = 0.170$, $X_3 = 0.250$, $X_4 = 0.334$, $X_5 = 0.416$) as marked on Figure 18(c) of the temperature profiles. Under uniform heating, as expected from the concept of traditional boundary layer flow, the boundary layer grows monotonously in the direction flow (rightward, as flow takes

**Notes:** (a) Uniform heating; (b) sinusoidal heating with $\phi = +90°$; (c) sinusoidal heating with $\phi = -90°$

place from the sidewalls to the center and here the left-half of the bottom is considered). For the present problem, the velocity boundary layer (δ_v) compared to the thermal boundary layer (δ_t) is relatively thinner (even with the uniform heating), which is expected with Pr <1. Both the thicknesses increase as Ra_m value decreases, irrespective of the mode of heating. However, under the sinusoidal heating, the thermal boundary layer thickness (δ_t) is markedly smaller than that of uniform heating [Figure 18(a)]. In case of velocity boundary layer thickness δ_v [in Figure 18(b)], compared to uniform heating, it is relatively higher. The enhanced heat transfer is because of relatively thinner thermal boundary layer, that in turn causes higher convective velocity and thicker velocity boundary layer. The waviness in boundary layer thicknesses results from uneven sinusoidal temperature distribution along the bottom wall.

4.6 Enhancement analysis
Finally, a comprehensive assessment of heat transfer enhancement through the sinusoidal heating is prepared using a parameter η (heat transfer parameter). It is defined with respect to the uniformly heated cavity as:
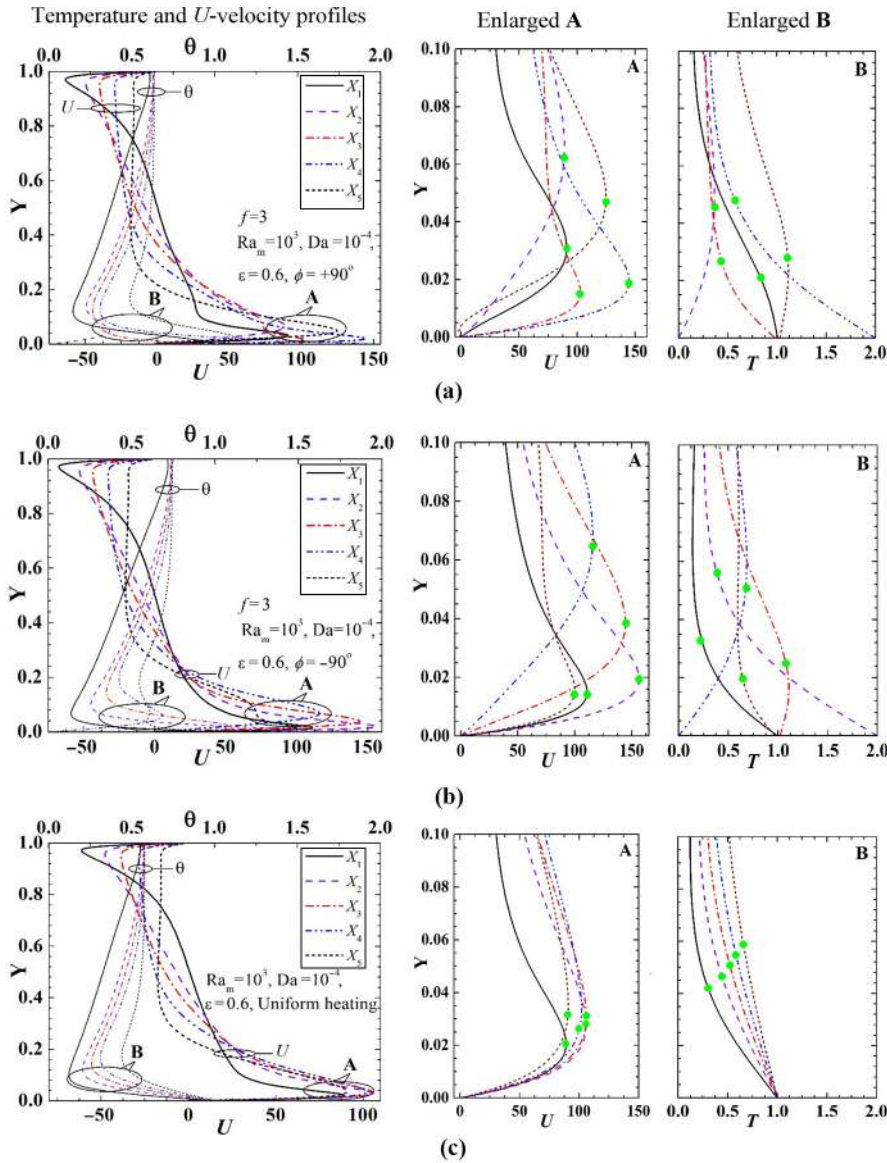
$$\eta = \frac{Nu_{sinusoidal\ heating}}{Nu_{isothermal\ heating}} \tag{13}$$
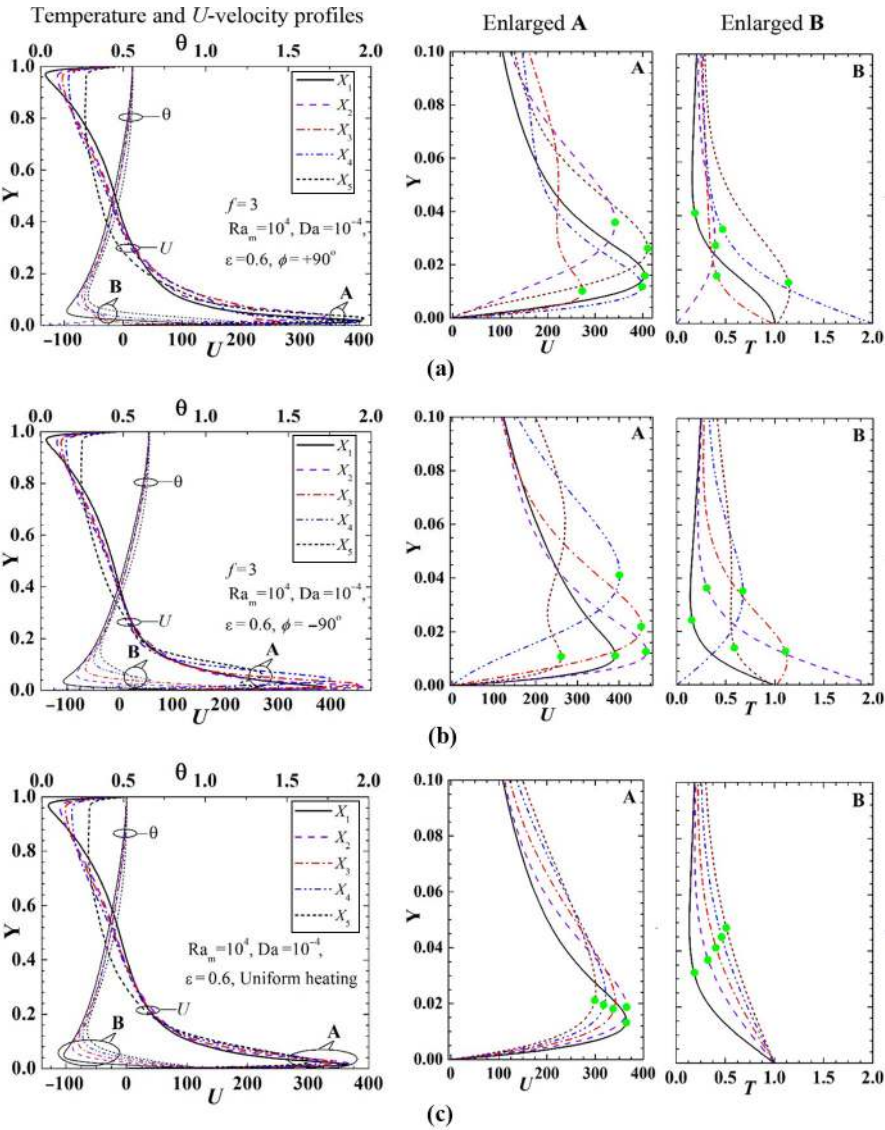
Figure 16.
Temperature profiles and U-velocity profiles for $Ra_m = 10^4$, $Da = 10^{-4}$ and $\varepsilon = 0.6$

Notes: (a) $f = 3$ and $\phi = +90°$; (b) $f = 3$ and $\phi = -90°$; (c) uniform heating. The locations of the profiles are: $X_1 = 0.0825$, $X_2 = 0.170$, $X_3 = 0.250$, $X_4 = 0.334$, $X_5 = 0.416$

By this definition, when η becomes greater than 1.0 indicate an augmentation in heat transfer. The magnitude of the enhancement is to be of $(\eta - 1) \times 100$ per cent. In Figure 19, both Nu and η are presented side by side to analyze heat transfer under different cases of heating (uniform, non-uniform) and the order of enhancement from multi-frequency

Figure 17.
Temperature profiles
and U-velocity
profiles for $Ra_m =$
10^3, $Da = 10^{-4}$ and
$\varepsilon = 0.6$

Notes: (a) $f = 3$ and $\phi = +90°$; (b) $f = 3$ and $\phi = -90°$; (c) uniform heating. The locations of
the profiles are: $X_1 = 0.0825$, $X_2 = 0.170$, $X_3 = 0.250$, $X_4 = 0.334$, $X_5 = 0.416$

sinusoidal heating. The analysis is presented keeping $Da = 10^{-4}$, $\varepsilon = 0.6$ and $I = 1$ as
constant.

It is observed that Nu is almost invariant up to $Ra_m = 30$ for uniform heating, 100 for
non-uniform with $\phi = +90°$ and 10 for non-uniform with $\phi = -90°$; thereafter, Nu

increases at higher rate with Ra_m till $Ra_m = 10^4$. The constant trend at lower Ra_m happens as thermal conduction dominates over convection in transporting heat from the bottom wall to the cold sidewalls of the cavity. In general when Ra_m increases above 10^2, Nu consistently increases with Ra_m irrespective of type of heating. Compared to uniform heating case, heat transfer for positive phase angle is always higher irrespective of frequency of heating. Furthermore, at lower Ra_m value the lower frequency is found more advantageous. The opposite trends are noted for negative phase angle, and the better heat transfer is observed when Ra_m exceeds 10^3. The plot of η in Figure 19 depicts the quantitative magnitude of heat transfer enhancement. The frequency rise changes the formation of thermal boundary layer potentially, which leads to enhanced heat transfer in the range of 52.55 to 62.25 per cent for
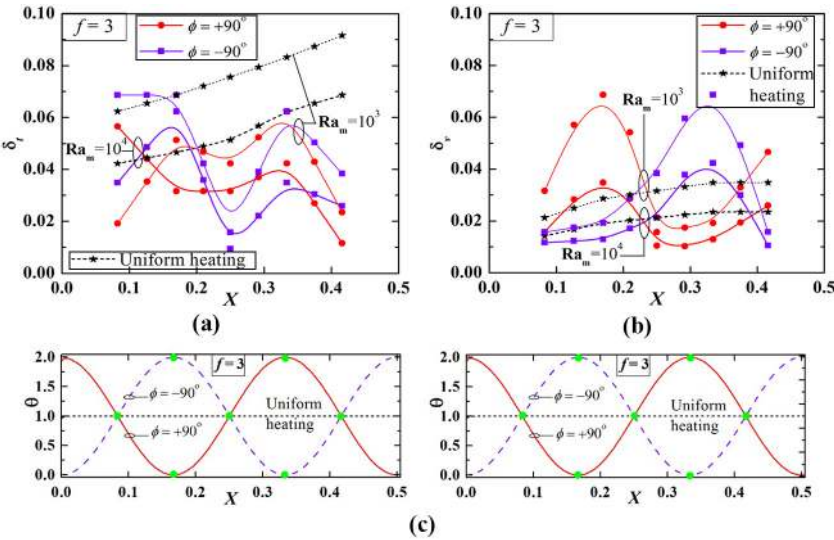
Figure 18.
Boundary layer thicknesses (δ_t, δ_v) near bottom wall at $f = 3$, $Da = 10^{-4}$, $\varepsilon = 0.6$ and $Ra_m = 10^4, 10^3$

Notes: (a) Temperature boundary layer; (b) velocity boundary layer; X-location of considered data-points is indicated on the temperature profiles in (c)
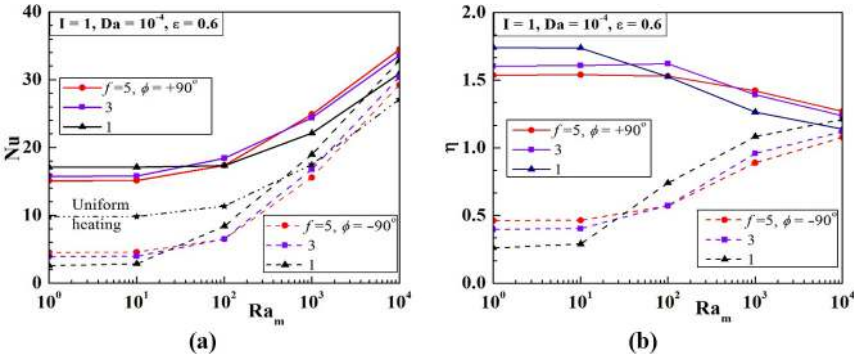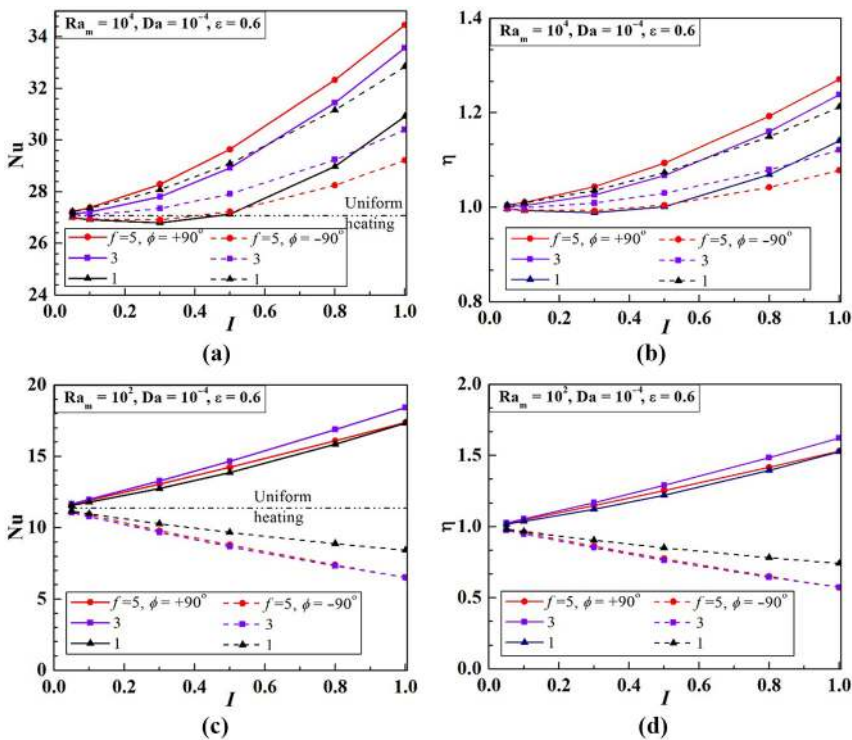

Figure 19.
Heat transfer analysis at fixed $Da = 10^{-4}$ and $\varepsilon = 0.6$

Notes: (a) Average Nusselt number; (b) heat transfer parameter

$\phi = +90°$; whereas it is in the range of 7.82 to 21.19 per cent for $\phi = -90°$. The enhanced heat transfer with increase in frequency happens through the intermediate cooling (or the rejection of heat from the cavity) as per the sine law of temperature profile along the bottom wall. The multi-frequency heating changes the shape, size and numbers of circulation cells (flow and energy) drastically. It should be noted here that the spatial frequency of temperature oscillation is limited in practical applications. However, from the fundamental viewpoint of analysis, the frequency in this work is taken up to $f = 5$, to illustrate the trend of heat transfer characteristics with the frequency rise and corresponding enhanced heat transfer compared to the uniform heating.

During multi-frequency sinusoidal heating apart from Ra_m and ϕ effects, the amplitude (I) of heating (temperature) is another important issue. This effect is explored in Figure 20 with different fixed Ra_m values at varied I. The average Nusselt number (Nu) is plotted against the amplitude (I) for various frequencies ($f = 1, 3, 5$) and phase angles ($\phi = \pm 90°$) keeping Da $= 10^{-4}$ and $\varepsilon = 0.6$ constant. In Figure 20(a) at $Ra_m = 10^4$, Nu increases monotonically with I irrespective of different f and ϕ. After $I = 0.5$, through sinusoidal heating increases heat transfer significantly compared to uniform heating. However, for each case, the maximum enhancement is noted at $I = 1$; the quantitative values of enhancements (η) for $\phi = +90°$ are 14.05, 23.86 and 27.82 per cent respectively for $f = 1, 3$ and 5. Whereas, the enhancements of η for the case of $\phi = -90°$ are 21.19, 12.14 and 7.82

Notes: (a) Average Nusselt number Nu at $Ra_m = 10^4$; (b) heat transfer parameter η for $Ram = 10^4$; (c) Nu at $Ra_m = 10^2$; (d) η for $Ra_m = 10^2$

Figure 20.
Impact of sinusoidal amplitude (I) at fixed Da $= 10^{-4}$, $\varepsilon = 0.6$ and different Ra_m

per cent, respectively for $f = 1$, 3 and 5. When the similar analysis is carried out at lower $Ra_m = 10^2$ in Figure 20(b), the impact of phase angles is greatly pronounced. Their effects on Nu become almost opposite as I increases; heat transfer at lower Ra_m markedly decreases at $\phi = -90°$. However for positive phase angle ($\phi = +90°$), Nu almost linearly increases with I. The enhancement in heat transfer becomes 52.55, 62.25 and 53.02 per cent for $f = 1$, 3 and 5, respectively.

5. Conclusions
The enhancement in heat transfer for natural convection is demonstrated in this work using spatially-varying sinusoidal heating for a bottom-heated porous cavity. For the proper judgement on the assessment of improved heat transfer (from the proposed non-uniform multi-frequency sinusoidal heating), the same mean-temperature of heating (such as a case of uniform heating) is considered as the reference for all the comparisons. The same mean-temperature could be an index of same heating load irrespective of the mode of heating. The underlying physics of the problem are systematically analyzed to explore the thermal convective flow and the energy transport in the cavity, using heatlines and boundary layer thicknesses. The impacts of involved parameters (such as Darcy–Rayleigh number Ra_m and the amplitude, frequency and phase angle φ of sinusoidal heating) are analyzed thoroughly for both the modes of uniform and non-uniform heating methods. The ranges of parameters for the positive outcomes (heat transfer enhancement) using sinusoidal heating are identified. The multi-frequency sinusoidal heating with positive phase angle is a superior heating strategy irrespective of Darcy–Rayleigh number. The negative phase angle at higher value of Ra_m ($>10^3$) could be effective. Depending upon the values of parameters and within the studied ranges, the natural convection heat transfer can be enhanced up to $\sim$74 per cent through multi-frequency sinusoidal heating. The present study has also demonstrated how to appreciate the thicknesses of hydrodynamic and thermal boundary layers numerically from the CFD predicted flow-fields of velocity and temperature.

The findings observed and the concept delivered here could be used for other thermal configurations or systems and can be extended to other areas of multi-physics (nanofluids, magneto-hydrodynamics, etc.) and heat transfer processes.

References

Anothe, B.V. and Lage, J.L. (1996), "Experimental investigation on pulsating horizontal heating of an enclosure filled with water", *Journal of Heat Transfer*, Vol. 118, pp. 889-896.

Bahrehmand, D. and Ameri, M. (2015), "Energy and exergy analysis of different solar air collector systems with natural convection", *Renewable Energy*, Vol. 74, pp. 357-368.

Baïri, A., Zarco-Pernia, E., de María, J.M.G. and, (2014), "A review on natural convection in enclosures for engineering applications: the particular case of the parallelogrammic diode cavity", *Applied Thermal Engineering*, Vol. 63 No. 1, pp. 304-322.

Banerjee, S., Mukhopadhyay, A. and Sen, S. (2008), "Natural convection in a bi-heater configuration of passive electronic cooling", *International Journal of Thermal Science*, Vol. 47 No. 11, pp. 1516-1527.

Bar-Cohen, A. (1987), "Thermal management of air and liquid-cooled multi-chip modules", *IEEE Transactions on Components, Hybrids, and Manufacturing Technology*, Vol. 10 No. 2, pp. 159-175.

Bhave, P., Narasimhan, A. and Rees, D.A.S. (2006), "Natural convection heat transfer enhancement using adiabatic block: optimal block size and Prandtl number effect", *International Journal of Heat and Mass Transfer*, Vol. 49 No. 21-22, pp. 3807-3818.

Biswas, N., Mahapatra, P.S. and Manna, N.K. (2016a), "Enhanced thermal energy transport using an adiabatic block inside lid driven cavity", *International Journal of Heat and Mass Transfer*, Vol. 100, pp. 407-427.

Biswas, N., Mahapatra, P.S. and Manna, N.K. (2016b), "Merit of non-uniform over uniform heating in a porous cavity", *International Communication in Heat and Mass Transfer*, Vol. 78, pp. 135-144.

Biswas, N., Mahapatra, P.S., Manna, N.K. and Roy, P.C. (2016c), "Influence of heater aspect ratio on natural convection in a rectangular enclosure", *Heat Transfer Engineering*, Vol. 37 No. 2, pp. 125-139.

Biswas, N., Manna, N.K., Datta, P. and Mahapatra, P.S. (2018), "Analysis of heat transfer and pumping power for bottom-heated porous cavity saturated with Cu-water nanofluid", *Powder Technology*, Vol. 326, pp. 356-369.

Calcagni, B., Marsili, F. and Paroncini, M. (2005), "Natural convective heat transfer in square enclosures heated from below", *Applied Thermal Engineering*, Vol. 25 No. 16, pp. 2522-2531.

Chamkha, A.J. (2002), "Double-diffusive convection in a porous enclosure with cooperating temperature and concentration gradients and heat generation or absorption effects", *Numerical Heat Transfer, Part A: Applications*, Vol. 41 No. 1, pp. 65-87.

Chamkha, A.J. and Khaled, A.R.A. (2000), "Similarity solutions for hydromagnetic mixed convection heat and mass transfer for hiemenz flow through porous media", *International Journal of Numerical Methods for Heat and Fluid Flow*, Vol. 10 No. 2, pp. 94-115.

Chamkha, A.J. and Rashad, A.M. (2012), "Natural convection from a vertical permeable cone in a nanofluid saturated porous media for uniform heat and nanoparticles volume fraction fluxes", *International Journal of Numerical Methods for Heat and Fluid Flow*, Vol. 22 No. 8, pp. 1073-1085.

Chamkha, A.J., Abbasbandy, S. and Rashad, A.M. (2015), "Non-Darcy natural convection flow for non-Newtonian nanofluid over cone saturated in porous medium with uniform heat and volume fraction fluxes", *International Journal of Numerical Methods for Heat and Fluid Flow*, Vol. 25 No. 2, pp. 422-437.

Cho, C.C., Yau, H.T. and Chen, C.K. (2012a), "Enhancement of natural convection heat transfer in a U-shaped cavity filled with Al_2O_3-water nanofluid", *Thermal Science*, Vol. 16 No. 5, pp. 1317-1323.

Cho, C.C., Yau, H.T. and Chen, C.K. (2012b), "Numerical investigation into natural convection heat transfer enhancement of copper-water nanofluid in a wavy wall enclosure", *Thermal Science*, Vol. 16 No. 5, pp. 1309-1316.

Das, D., Roy, M. and Basak, T. (2017), "Studies on natural convection within enclosures of various (non-square) shapes – a review", *International Journal of Heat and Mass Transfer*, Vol. 106, pp. 356-406.

Datta, P., Mahapatra, P.S., Ghosh, K., Manna, N.K. and Sen, S. (2016), "Heat transfer and entropy generation in a porous square enclosure in presence of an adiabatic block", *Transport in Porous Media*, Vol. 111 No. 2, pp. 305-329.

de Vahl Davis, G. (1983), "Natural convection of air in a square cavity: a bench mark numerical solution", *International Journal for Numerical Methods in Fluids*, Vol. 3 No. 3, pp. 249-264.

Deng, Q.H. and Chang, J.J. (2008), "Natural convection in a rectangular enclosure with sinusoidal temperature distributions on both side walls", *Numerical Heat Transfer, Part A*, Vol. 54 No. 5, pp. 507-524.

Due, Z.D. and Bilgen, E. (1990), "Effects of heat intensity, size, and position of the components on temperature distribution within an electronic PCB enclosure", *Journal of Electronic Packaging*, Vol. 112 No. 3, pp. 249-254.

Garimella, S.V., Persoons, T., Weibel, J.A. and Gektin, V. (2016), "Electronics thermal management in information and communications technologies: challenges and future directions", *EEE Transactions on Components, Packaging and Manufacturing Technology*, pp. 1-15.

Ghalambaz, M., Jamesahar, E., Ismael, M.A. and Chamkha, A.J. (2017), "Fluid-structure interaction study of natural convection heat transfer over a flexible oscillating fin in a square cavity", *International Journal of Thermal Science*, Vol. 111, pp. 256-273.

Haghighi, A.P. and Maerefat, M. (2014), "Solar ventilation and heating of buildings in sunny winter days using solar chimney", *Sustainable Cities and Society*, Vol. 10, pp. 72-79.

Hwang, M.L. and Yang, Y.T. (2012), "Numerical simulation of turbulent fluid flow and heat transfer characteristics in metallic porous block subjected to a confined slot jet", *International Journal of Thermal Sciences*, Vol. 55, pp. 31-39.

Incropera, F.P. (1988), "Convection heat transfers in electronic equipment cooling", *Journal of Heat Transfer*, Vol. 110 No. 4b, pp. 1097-1111.

Ismael, M.A., Armaghani, T. and Chamkha, A.J. (2014a), "Conjugate heat transfer and entropy generation in a cavity filled with a nanofluid-saturated porous media and heated by a triangular solid", *Journal of the Taiwan Institute of Chemical Engineers*, Vol. 59, pp. 138-151.

Ismael, M.A., Pop, I. and Chamkha, A.J. (2014b), "Mixed convection in a lid-driven square cavity with partial slip", *International Journal of Thermal Sciences*, Vol. 82, pp. 47-615.

Lauriat, G. and Prasad, V. (1989), "Non-Darcian effects on natural convection in a vertical porous enclosure", *International Journal of Heat and Mass Transfer*, Vol. 32 No. 11, pp. 2135-2148.

Kalidasan, K., Velkennedy, R. and Kanna, P.R. (2016), "Natural convection heat transfer enhancement using nanofluid and time-variant temperature on the square enclosure with diagonally constructed twin adiabatic blocks", *Applied Thermal Engineering*, Vol. 92, pp. 219-235.

Kasayapanand, N. and Kiatsiriroat, T. (2009), "Enhanced heat transfer in partially open square cavities with thin fin by using electric field", *Energy Conversion and Management*, Vol. 50 No. 2, pp. 287-296.

Khaled, A.R.A. and Vafai, K. (2003), "The role of porous media in modeling flow and heat transfer in biological tissues", *International Journal of Heat and Mass Transfer*, Vol. 46 No. 26, pp. 4989-5003.

Khanafer, K., Vafai, K. and Kangarlu, A. (2003), "Water diffusion in biomedical systems as related to magnetic resonance imaging", *Magnetic Resonance Imaging*, Vol. 21 No. 1, pp. 17-31.

Khanafer, K., Vafai, K. and Lightstone, M. (2003), "Buoyancy-driven heat transfer enhancement in a two-dimensional enclosure utilizing nanofluids", *International Journal of Heat and Mass Transfer*, Vol. 46 No. 19, pp. 3639-3653.

Khandelwal, M.K., Bera, P. and Chakrabarti, A. (2012), "Influence of periodicity of sinusoidal bottom boundary condition on natural convection in porous enclosure", *International Journal of Heat and Mass Transfer*, Vol. 55 Nos 11/12, pp. 2889-2900.

Kheirabadi, A.C. and Groulx, D. (2016), "Cooling of server electronics: a design review of existing technology", *Applied Thermal Engineering*, Vol. 105, pp. 622-638.

Kim, S.J. and Jang, S.P. (2002), "Effects of the Darcy number, the Prandtl number, and the Reynolds number on local thermal non-equilibrium", *International Journal of Heat and Mass Transfer*, Vol. 45 No. 19, pp. 3885-3896.

Kimura, S. and Bejan, A. (1983), "The heatline visualization of convective heat transfer", *Journal of Heat Transfer*, Vol. 105 No. 4, pp. 916-919.

Kota, K., Burton, L. and Joshi, Y. (2012), "Performance of an air-cooled heat sink with microscale dimples under transitional flow conditions", *13th Inter Society Conference on Thermal and Thermomechanical Phenomena in Electronic Systems*, pp. 450-456.

Kwak, H.S., Kuwahara, K. and Hyun, J.M. (1998), "Resonant enhancement of natural convection heat transfer in a square enclosure", *International Journal of Heat and Mass Transfer*, Vol. 41 No. 18, pp. 2837-2846.

Mahapatra, P.S, De, S., Ghosh, K., Manna, N.K. and Mukhopadhyay, A. (2013), "Heat transfer enhancement and entropy generation in a square enclosure in the presence of adiabatic and isothermal blocks", *Numerical Heat Transfer, Part A*, Vol. 64 No. 7, pp. 577-596.

Mahapatra, P.S., Manna, N.K., Ghosh, K. and Mukhopadhyay, A. (2015), "Heat transfer assessment of an alternately active bi-heater undergoing transient natural convection", *International Journal of Heat and Mass Transfer*, Vol. 83, pp. 450-464.

Mahapatra, P.S., Chatterjee, S., Mukhopadhyay, A., Manna, N.K. and Ghosh, K. (2016), "Proper orthogonal decomposition of thermally-induced flow structure in an enclosure with alternately active localized heat sources", *International Journal of Heat and Mass Transfer*, Vol. 94, pp. 373-379.

Mahapatra, P.S., Mukhopadhyay, A., Manna, N.K. and Ghosh, K. (2018), "Heatlines and other visualization techniques for confined heat transfer systems", *International Journal of Heat and Mass Transfer*, Vol. 118, pp. 1069-1079.

Mandal, D.K., Manna, N.K. and Chakrabarti, S. (2010), "Numerical study of blood flow through different double bell-shaped stenosed coronary artery during the progression of the disease, atherosclerosis", *International Journal of Numerical Methods for Heat and Fluid Flow*, Vol. 20 No. 6, pp. 670-698.

Mondal, M.K., Manna, N.K. and Saha, R. (2014), "Study of leakage flow through a spool valve under blocked-actuator port condition – simulation and experiment", *Proceedings of the Institution of Mechanical Engineers, Part C*, Vol. 228 No. 8, pp. 1405-1417.

Meng, X., Wang, Y., Wang, J. and Long, E. (2016), "Effect of periodically alternating wall temperature on natural convection heat transfer enhancement in a square cavity filled with Cu-water nanofluids", *Heat Transfer Research*, Vol. 47 No. 9, pp. 839-854.

Nagendran, B., Raghupathy, A. and Maltz, W. (2015), "Thermal management challenges in forced convection tablets", *31st Thermal Measurement, Modeling and Management Symposium (SEMI-THERM)*, pp. 37-40.

Narasimham, G.S.V.L. (2010), "Natural convection from discrete heat sources in enclosures: an overview", *Vivechan International Journal of Research*, Vol. 1, pp. 63-78.

Nield, D.A. and Bejan, A. (2006), *Convection in Porous Media*, 3rd ed., Springer, Berlin.

Ostrach, S. (1988), "Natural convection in enclosures", *Journal of Heat Transfer*, Vol. 110 No. 4b, pp. 1175-1190.

Oztop, H.F., Abu-Nada, E., Varol, Y. and Al-Salem, K. (2011), "Computational analysis of nonisothermal temperature distribution on natural convection in nanofluid filled enclosures", *Superlattices and Microstructures*, Vol. 49 No. 4, pp. 453-467.

Öztop, H.F., Estellé, P., Yan, W.M., Al-Salem, K., Orfi, J. and Mahian, O. (2015), "A brief review of natural convection in enclosures under localized heating with and without nanofluids", *International Communication in Heat and Mass Transfer*, Vol. 60, pp. 37-44.

Papanicolaou, E. and Gopalakrishna, S. (1995), "Natural convection in shallow, horizontal layers encountered in electronic cooling", *Journal of Electronic Packaging*, Vol. 117 No. 4, pp. 307-316.

Parvin, S. and Chamkha, A.J. (2014), "An analysis on free convection flow, heat transfer and entropy generation in an odd-shaped cavity filled with nanofluid", *International Communications in Heat and Mass Transfer*, Vol. 3, pp. 8-17.

Patankar, S.V. (1980), *Numerical Heat Transfer and Fluid Flow*, Hemisphere, New York, NY.

Pop, I. and Ingham, D.B. (Eds) (2002), *Transport Phenomena in Porous Media*, Vol. 2, Pergamon, Oxford.

Ramakrishna, D., Basak, T., Roy, S. and Pop, I. (2013), "Analysis of heatlines during natural convection within porous square enclosures: effects of thermal aspect ratio and thermal boundary conditions", *International Journal of Heat and Mass Transfer*, Vol. 59, pp. 206-218.

Remsburg, R. (2001), *Thermal Design of Electronic Equipment*, CRC Press LLC, Boca Raton, FL.

Saeid, N.F. (2005), "Natural convection in porous cavity with sinusoidal bottom wall temperature variation", *International Communication in Heat and Mass Transfer*, Vol. 32 No. 3-4, pp. 454-463.

Saravanan, S. and Sivaraj, C. (2011), "Natural convection in an enclosure with a localized nonuniform heat source on the bottom wall", *International Journal of Heat and Mass Transfer*, Vol. 54 No. 13-14, pp. 2820-2828.

Sarris, I.E., Lekakis, I. and Vlachos, N.S. (2002), "Natural convection in a 2D enclosure with sinusoidal upper wall temperature", *Numerical Heat Transfer, Part A*, Vol. 42 No. 5, pp. 513-530.

Sekyere, C.K.K., Forson, F.K. and Adam, F.W. (2016), "Experimental investigation of the drying characteristics of a mixed mode natural convection solar crop dryer with back up heater", *Renewable Energy*, Vol. 92, pp. 532-542.

Selimefendigil, F. and Öztop, H.F. (2016), "Conjugate natural convection in a cavity with a conductive partition and filled with different nanofluids on different sides of the partition", *Journal of Molecular Liquids*, Vol. 216, pp. 67-77.

Sharif, M.A.R. and Mohammad, T.R. (2005), "Natural convection in cavities with constant flux heating at the bottom wall and isothermal cooling from the sidewalls", *International Journal of Thermal Science*, Vol. 44 No. 9, pp. 865-878.

Sheikholeslami, M., Gorji-Bandpy, M., Ganji, D.D. and Soleimani, S. (2014), "MHD natural convection in a nanofluid filled inclined enclosure with sinusoidal wall using CVFEM", *Neural Computing and Applications*, Vol. 24 No. 3-4, pp. 873-882.

Sheremet, M.A. and Pop, I. (2014), "Natural convection in a square porous cavity with sinusoidal temperature distributions on both side walls filled with a nanofluid: Buongiorno's mathematical model", *Transport in Porous Media*, Vol. 105 No. 2, pp. 411-429.

Sivasankaran, S. and Bhuvaneswari, M. (2013), "Natural convection in a porous cavity with sinusoidal heating on both sidewalls", *Numerical Heat Transfer, Part A*, Vol. 63 No. 1, pp. 14-30.

Tagawa, T. and Ozoe, H. (1997), "Enhancement of heat transfer rate by application of a static magnetic field during natural convection of liquid metal in a cube", *Journal of Heat Transfer*, Vol. 119 No. 2, pp. 265-271.

Tasnim, S.H. and Collins, M.R. (2004), "Numerical analysis of heat transfer in a square cavity with a baffle on the hot wall", *International Communication in Heat and Mass Transfer*, Vol. 31, pp. 639-650.

Valencia, A. and Frederick, R.L. (1989), "Heat transfer in square cavities with partially active vertical walls", *International Journal of Heat and Mass Transfer*, Vol. 8, pp. 1567-1574.

Varol, Y., Oztop, H.F. and Pop, I. (2008), "Numerical analysis of natural convection for a porous rectangular enclosure with sinusoidally varying temperature profile on the bottom wall", *International Communication in Heat and Mass Transfer*, Vol. 35 No. 1, pp. 56-64.

Versteeg, H.K. and Malalasekera, W. (1995), *An Introduction to Computational Fluid Dynamics: The Finite Volume Method*, Longman Scientific and Technical.

Wu, F., Wang, G. and Zhou, W. (2016), "Buoyancy induced convection in a porous cavity with sinusoidally and partially thermally active sidewalls under local thermal non-equilibrium condition", *International Communication in Heat and Mass Transfer*, Vol. 75, pp. 100-114.

Zhao, C.Y. (2012), "Review on thermal transport in high porosity cellular metal foams with open cells", *International Journal of Heat and Mass Transfer*, Vol. 55 Nos 13/14, pp. 3618-3632.

Zhang, D.J., Zhang, H., Liu, D., Zhao, F.Y. and Wang, H.Q. (2016), "Conjugate thermal transport enhancement for an air filled enclosure with heat conducting partitions using inverse convection methodology", *International Journal of Heat and Mass Transfer*, Vol. 102, pp. 788-800.

Zhang, X.W. and Liu, W. (2008), "New criterion for local thermal equilibrium in porous media", *Journal of Thermophysics and Heat Transfer*, Vol. 22 No. 4, pp. 649-653.

Corresponding author
Nirmal Kumar Manna can be contacted at: nirmalkmannaju@gmail.com